

Neural Approaches for Multi-Objective Routing on Multigraphs

Filip Rydin¹, Attila Lischka¹, Jiaming Wu¹, Morteza Haghiri Chehreghani², Balázs Kulcsár¹

¹ Chalmers University of Technology, Sweden

² Chalmers University of Technology & University of Gothenburg, Sweden
{filipry, lischka, jiaming.wu, morteza.chehreghani, kulcsar}@chalmers.se

Abstract

Learning-based methods for routing have gained significant attention in recent years, both in single-objective and multi-objective contexts. Yet, existing methods are unsuitable for routing on multigraphs, which feature multiple edges with distinct attributes between node pairs, despite their strong relevance in real-world scenarios. In this paper, we propose two graph neural network-based methods to address multi-objective routing on multigraphs. Our first approach operates directly on the multigraph by autoregressively selecting edges until a tour is completed. The second model first simplifies the multigraph via a learned pruning strategy and then performs routing on the resulting simple graph. We evaluate both models empirically and demonstrate their strong performance across a range of problems and distributions¹.

1 Introduction

Routing problems, including the well-known Traveling Salesman Problem (TSP), are central for optimizing operations in modern transport systems. A key assumption is often that an optimal path can be selected beforehand between each pair of locations. However, in reality, several paths may exist that cannot be chosen between a priori. This naturally leads to a multigraph representation. Notably, by planning on a multigraph rather than a simple graph, Ben Ticha et al. (2017) demonstrated a cost reduction of up to 10.5% for the vehicle routing problem with time-windows. Similarly Lai, Caliskan Demirag, and Leung (2016) demonstrated average savings of circa 5% for a heterogeneous vehicle routing problem. Such results can be pivotal in for instance last-mile-delivery, which accounts for 41% of total supply chain cost according to Capgemini Research Institute (2023).

Yet, routing problems on simple graphs are already difficult to solve, especially in real-time, as they are generally NP-hard. The multigraph setup further increases this complexity. Moreover, such a framework is particularly interesting in the Multi-Objective (MO) case, where each edge may be associated with several conflicting cost criteria, such as time, distance or energy. MO routing is typically harder, as the number of Pareto optimal solutions can grow exponentially with the size of the problem (Ehr Gott and Gandibleux 2000). Clearly, MO routing on multigraphs poses significant

challenges, while remaining highly relevant for real-world applications.

Recently, however, learning-based methods have emerged as promising options for routing, offering speed, accuracy, and broad applicability across problems (Kool, van Hoof, and Welling 2018; Drakulic, Michel, and Andreoli 2025). Yet, current approaches are designed for simple graphs and not suited for the multigraph representation. This is especially true in the MO setting, where neural approaches have demonstrated excellent results on Euclidean instances (Lin, Yang, and Zhang 2022; Fan et al. 2025), but lack support even for asymmetric graphs, in spite of their higher practical relevance (Boyacı, Dang, and Letchford 2021).

We attempt to bridge the gap between learning-based methods for MO routing and accurate network representations. Concretely, our main contributions are:

- We design models to handle multigraph inputs, where not only the next node but also the edge must be selected. To our knowledge, we present the first neural solvers designed for such input structures. Although we deal with MO optimization, our approach can be highly useful in single-objective cases too.
- Our models are also capable of handling a variety of MO routing problems on asymmetric graphs. In contrast, current neural MO methods are either problem-specific or designed exclusively for the Euclidean setting, where edge costs are symmetric and determined only by the node coordinates.
- We propose two separate models based on Graph Neural Networks (GNNs): One edge-based working directly on the multigraph and one dual-task model that first prunes the multigraph into a simple graph and then selects routes. The former is simple but slow while the latter is more complex but faster.
- Experimentally, we show that our approach achieves competitive results for several MO routing problems on asymmetric graphs and multigraphs.

2 Related Work

2.1 Learning for Routing

Motivated by the success of end-to-end learning in fields such as image classification and language modeling, neural

¹Our code will be released publicly upon paper acceptance.

solutions for routing have gained increasing attention during the last years. Broadly, methods can be classified by how they obtain tours. Two prominent alternatives are *autoregressive construction*, based on iterative building of tours one node at a time, and *non-autoregressive construction*, that outputs heatmaps in a one-shot fashion for down-stream decoding with some search method. Examples from the first category include Vinyals, Fortunato, and Jaitly (2015); Kool, van Hoof, and Welling (2018); Kwon et al. (2020). Examples from the second category are Joshi, Laurent, and Bresson (2019); Fu, Qiu, and Zha (2021); Sun and Yang (2023). For a more comprehensive discussion of these methods, we refer the reader to Appendix A, which presents additional related work.

The literature on MO routing is more sparse than in the single-objective case. A key contribution was made by Lin, Yang, and Zhang (2022), who proposed an autoregressive construction approach using a single neural model to learn the Pareto set of solutions. Regarding asymmetric problems, the only existing learning-based methods we are aware of are those introduced by Santiyuda et al. (2024) and Zhou, Kong, and Wang (2025). However, both these approaches are tailored to specific problems and have been evaluated within narrowly defined domains. In contrast, our method is capable of addressing a broad class of routing problems and is evaluated across various problems and settings.

2.2 Routing on Multigraphs

The multigraph representation has become more and more common for MO shortest path problems during recent years (Weiszer, Burke, and Chen 2020; Beke, Weiszer, and Chen 2021). Such a framework has also been applied to combinatorial routing problems like Vehicle Routing Problems (VRPs), but to a lower extent. Garaix et al. (2010) performed the first study in this regard and later works include Lai, Caliskan Demirag, and Leung (2016); Ben Ticha et al. (2017); Tikani, Setak, and Demir (2021).

A common theme across these studies is that the multigraph representation leads to considerably improved solutions, while simultaneously increasing the complexity of these already difficult problems. Consequently, learning-based methods should be able to fill a clear need for new solvers in this area, as they have proven to be efficient, effective and broadly applicable. To the best of our knowledge, this work presents the first learning-based approach to address combinatorial routing problems such as the TSP and VRPs on multigraphs.

3 Problem Formulation

We define a general multi-objective routing problem as

$$\min_{\pi \in \Pi} f(\pi), \quad (1)$$

where $f : \Pi \rightarrow \mathbb{R}^m$ with $m > 1$. Here, $\pi \in \Pi$ represents a feasible route in the multigraph G , encoded as a sequence of edges, and $f(\pi)$ is the associated cost vector. Due to the combinatorial nature of the feasible solution space Π and the multiple conflicting objectives, the problem is generally NP-hard.

The solution to an MO routing problem is a set of objective values known as the Pareto Front (PF) with associated routes in the Pareto Set (PS). Formally, we define the PS as

$$\text{PS} := \{\pi \in \Pi \mid \nexists \pi' \in \Pi : f(\pi') \prec f(\pi)\}, \quad (2)$$

where $f(\pi') \prec f(\pi)$ denotes that $f(\pi')$ dominates $f(\pi)$, meaning

$$\begin{aligned} f_i(\pi') &\leq f_i(\pi) \quad \forall i = 1, \dots, m, \\ f_i(\pi') &< f_i(\pi) \text{ for at least one } i. \end{aligned} \quad (3)$$

Correspondingly, the Pareto Front (PF) is defined as the image of the Pareto Set under f , that is,

$$\text{PF} := \{f(\pi) \in \mathbb{R}^m \mid \pi \in \text{PS}\}. \quad (4)$$

Intuitively, the PS represents solutions for which no strictly better alternative exists.

To obtain this set, we utilize a typical method: decomposition through scalarization. The idea is to translate the MO problem into several subproblems that can be solved separately. Let $\lambda \in \mathbb{R}^m$ such that $\lambda_i \geq 0 \forall i$ and $\sum_i \lambda_i = 1$ be a vector that controls the preference among the objectives. Then, under *Linear Scalarization* (LS), the single-objective cost is $f_\lambda(\pi) = \sum_i \lambda_i f_i(\pi)$ and the corresponding subproblem is $\min_{\pi} f_\lambda(\pi)$. Unfortunately, it is well-known that there may be solutions in the PS that do not solve an LS subproblem for any preference λ (Ehrgott 2005). The *Chebyshev scalarization* has more favorable properties. Let z_i^* be an ideal value for objective i . Then, the Chebyshev scalarized cost is

$$f_\lambda(\pi) = \max_i \{\lambda_i |f_i(\pi) - z_i^*|\}. \quad (5)$$

Given a solution in the PS, there always exists a preference λ and corresponding Chebyshev subproblem for which the solution is optimal (Choo and Atkins 1983).

In our context of multigraphs, it is interesting to consider how problems simplify under scalarization. We highlight an important result for the Multi-Objective TSP (MOTSP), in which the total cost of a tour is the sum of the vectorial costs of the traversed edges. The proof of the following proposition is omitted due to its simplicity. Given a linear scalarization defined by a preference vector λ , define the reduced graph $G(\lambda)$ by removing any edge whose scalarized cost is strictly worse than that of a parallel edge.

Proposition 1. *Let $f_\lambda(\pi)$ denote the linearly scalarized cost and let $\Pi(\lambda) \subset \Pi$ be the set of feasible tours on the pruned graph $G(\lambda)$. Then, the optimal value of the scalarized subproblem is preserved:*

$$\min_{\pi \in \Pi} f_\lambda(\pi) = \min_{\pi \in \Pi(\lambda)} f_\lambda(\pi). \quad (6)$$

This illustrates that a multigraph representation is sometimes easy to handle using pruning. However, under Chebyshev scalarization or for more complex problems (e.g., with edge attributes that contribute nonlinearly to the cost), similar results might not be available. As such, we propose to learn which parallel edge is optimal while simultaneously learning to construct the optimal route for each preference λ . Moreover, by explicitly taking into account the multigraph representation when designing our models, we obtain better results and faster inference than if we pre-prune the multigraphs, even for the MOTSP.

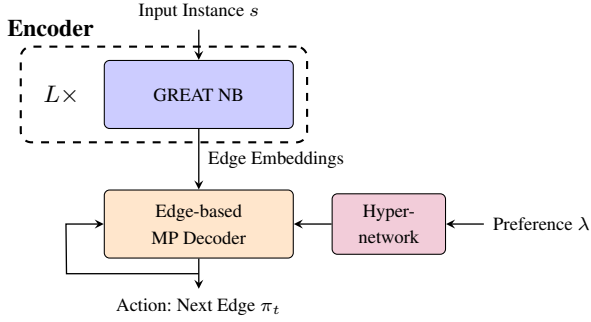


Figure 1: Edge-Based GMS

4 GNN-Based Multigraph Solver

In the following, we propose two approaches based on GNNs for solving MO multigraph routing problems. We call our method GNN-based Multigraph Solver (GMS) and propose an edge-based variant constructing routes autoregressively directly on the multigraph as well as a variant with two decoders that first prunes and then constructs routes.

Both variants require an encoder that i) can handle input data structured as multigraphs and ii) works with and outputs edge embeddings. While there are multiple GNN architectures that fit this description, we utilize the Graph Edge Attention Network (GREAT) of Lischka et al. (2025), since it has been applied in an autoregressive framework and shown competitive performance for non-Euclidean single-objective routing problems.

Specifically, we utilize the Node-Based (NB) version of GREAT. We refer the reader to Lischka et al. (2025) for details. Here, it suffices to say that the core component of an NB GREAT-layer is an attention sublayer, that utilizes attention scores α' and α'' to compute a temporary node-feature x for each node i according to

$$x_i = \left(\sum_{l \in E^+(i)} \alpha'_{il} W'_1 e_l \parallel \sum_{l' \in E^-(i)} \alpha''_{il'} W''_1 e_{l'} \right). \quad (7)$$

Here, \parallel is the concatenation operation, e_l denotes an edge embedding for edge l , W'_1 and W''_1 are trainable weight matrices and $E^+(i)$, $E^-(i)$ denote outgoing and incoming edges respectively. New edge embeddings are then computed according to

$$e'_l = W_2 (x_{\text{start}(l)} \parallel x_{\text{end}(l)}), \quad (8)$$

where $\text{start}(l)$ and $\text{end}(l)$ denote the start and end nodes of the directed edge l . The attention layers are arranged into a single GREAT-layer together with feed-forward layers, residual connections and normalization according to the original transformer architecture (Vaswani et al. 2017). Note that the residual connections are important as they allow parallel edges to have differing embeddings.

4.1 Edge-Based GMS

Vanilla node-based construction is insufficient for our purpose, as it relies on predicting the next node in the route,

while we also require an edge-selection between the current node and the next. Thus, we propose an end-to-end edge-based model that instead predicts the next edge, and thereby implicitly the next node. We call this Edge-based GMS (GMS-EB).

We visualize GMS-EB in Figure 1. The encoder, consisting of L GREAT-layers, outputs edge embeddings. Using them, the decoder constructs valid tours autoregressively. Given the instance s and incomplete route $\pi_{1:t-1}$ in construction step t , the decoder selects edge π_t with probability $p_{\theta(\lambda)}(\pi_t \mid \pi_{1:t-1}, s)$. Thus the probability of the whole route π is

$$p_{\theta(\lambda)}(\pi \mid s) = \prod_{t=1}^T p_{\theta(\lambda)}(\pi_t \mid \pi_{1:t-1}, s). \quad (9)$$

Here, $\theta(\lambda)$ is the weights of the model given the current preference λ . As Navon et al. (2021) and Lin, Yang, and Zhang (2022), we utilize a Multi-Layer Perceptron (MLP) hyper-network to preference-condition the decoder, while keeping the encoder preference-agnostic. Consequently we form the decoder weights according to $\theta_{\text{dec}}(\lambda) = \text{MLP}(\lambda)$ and set

$$\theta(\lambda) = [\theta_{\text{enc}}, \theta_{\text{dec}}(\lambda)]. \quad (10)$$

Regarding the decoder architecture, it is an edge-based variant of the Multi-Pointer (MP) decoder from Jin et al. (2023). We detail this component further in Appendix B.

Note that a multigraph with N nodes and M edges between each pair of nodes has $\mathcal{O}(MN^2)$ edges in total. Moreover, the decoder must be run $\mathcal{O}(N)$ times to construct a full tour and we roll out $\mathcal{O}(N)$ sample trajectories according to the POMO framework (Kwon et al. 2020). Hence, an edge-based decoder scales as $\mathcal{O}(MN^4)$ compared to a node-based one that scales as $\mathcal{O}(N^3)$. Consequently, we propose a second architecture that employs a node-based decoder and thereby scales better to higher node counts in terms of memory requirements and runtime.

4.2 Dual Head GMS

For a node-based decoder, we need to ensure that the action of choosing a node uniquely defines which edge to choose. This is achieved by pruning parallel edges, leaving a unique one between each node pair. In general, choosing this edge is not trivial. As such, we propose to learn the choice using a dual decoder setup.

We call this approach Dual Head GMS (GMS-DH) and it is visualized in Figure 2. The key is that we insert another decoder before the final GREAT layer, which uses intermediate edge embeddings to select the parallel edge to keep. Let E_{ij} be the set of edges between the node pair (i, j) . The selection-decoder produces the probability $q_{\tilde{\theta}(\lambda)}(l \mid i, j, s)$ of retaining $l \in E_{ij}$. As we treat each node pair independently and select one edge per pair, the probability of the joint selection \mathcal{E} of active edges is

$$q_{\tilde{\theta}(\lambda)}(\mathcal{E} \mid s) = \prod_{l \in \mathcal{E}} q_{\tilde{\theta}(\lambda)}(l \mid \text{start}(l), \text{end}(l), s). \quad (11)$$

Again, the weights $\tilde{\theta}(\lambda)$ are generated by an MLP hyper-network. We detail the architecture for the selection-decoder further in Appendix B.

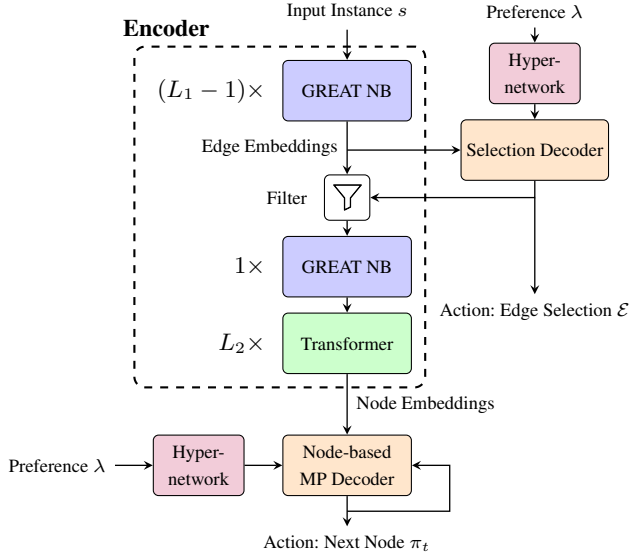


Figure 2: Dual Head GMS

The edge choice from the first decoder is fed back into the encoder, where the embeddings of corresponding edges are aggregated into node embeddings using (7). After this final GREAT layer, we find it beneficial to add a small number of standard transformer layers to obtain more expressive node embeddings for the second decoder, which constructs routes.

The routing-decoder is a preference-conditioned version of the multi-pointer decoder (Jin et al. 2023). Similarly to the edge-based version above, given the partial tour $\pi_{1:t-1}$, this decoder outputs the probabilities $p_{\theta(\lambda)}(\pi_t | \pi_{1:t-1}, s, \mathcal{E})$ for the next construction step, where π_t now denotes a node and the probability depends on the edge choice \mathcal{E} .

Remark that when applying GMS-DH to simple graphs, we simply remove the first decoder. Also note that this architecture ensures that the first $L_1 - 1$ layers only need to be run once for each instance as they are preference-agnostic and utilize the entire multigraph. This reduces the runtime compared to letting the encoder be preference-aware or pruning the multigraph for each preference before encoding.

From a broader perspective, our approach in GMS-DH can be viewed as a combination of non-autoregressive and autoregressive construction. As a drawback, the edge choice can no longer depend on the context given by the partial tour. Instead, it must be chosen before starting roll-out.

4.3 Training Algorithm

Our first proposed model, GMS-EB, is trained using the Multi-Objective REINFORCE from Lin, Yang, and Zhang (2022). Given a preference $\lambda \sim \Lambda$ and instance $s \sim S$, the model parameterizes a policy $p_{\theta(\lambda)}(\cdot | s)$ according to (9). A tour π is associated with a Chebyshev reward corresponding to the negative scalarized cost (5):

$$R_\lambda(\pi) = -\max_i \{\lambda_i | f_i(\pi) - z_i^*\}. \quad (12)$$

The objective during training is to maximize

$$J(\theta) = \mathbb{E}_{\pi \sim p_\theta, \lambda \sim \Lambda, s \sim S} [R_\lambda(\pi)]. \quad (13)$$

To stabilize the training, we form a baseline $b_\lambda(s_i)$ by rolling out K tours for the same instance s_i and averaging the reward, according to the POMO framework (Kwon et al. 2020). The policy gradient is then utilized to update the model weights and it is approximated, given one preference λ , according to

$$\nabla J(\theta) \approx \frac{1}{BK} \sum_{i,j=1}^{B,K} A_{ij} \nabla_\theta \log(p_{\theta(\lambda)}(\pi_{ij} | s_i)), \quad (14)$$

where B is the batch size of instances and the advantage is

$$A_{ij} = R_\lambda(\pi_{ij}) - b_\lambda(s_i). \quad (15)$$

For the second model, the training is more involved. Given an edge selection $\mathcal{E} \sim q_{\tilde{\theta}(\lambda)}$ from the selection-head according to (11), the routing-head parameterizes a policy $p_{\theta(\lambda)}(\cdot | s, \mathcal{E})$ and obtains a scalar reward $R_\lambda^{(2)}(\pi) = R_\lambda(\pi)$ by (12) as usual. With a fixed $\tilde{\theta}$, the objective for this head is to maximize

$$J_2(\theta) = \mathbb{E}_{\pi \sim p_\theta, \lambda \sim \Lambda, s \sim S, \mathcal{E} \sim q_{\tilde{\theta}}} [R_\lambda^{(2)}(\pi)]. \quad (16)$$

On the other hand, the task of the selection-head is to ensure that the edge choice is optimal. Let $\tilde{\pi}(\mathcal{E})$ denote the optimal tour on the pruned graph given selection \mathcal{E} . Then, define the reward and objective function based on the optimal tour according to

$$R_\lambda^{(1)}(\mathcal{E}) = R_\lambda(\tilde{\pi}(\mathcal{E})), \quad (17)$$

$$J_1(\tilde{\theta}) = \mathbb{E}_{\lambda \sim \Lambda, s \sim S, \mathcal{E} \sim q_{\tilde{\theta}}} [R_\lambda^{(1)}(\mathcal{E})].$$

As the optimal tour $\tilde{\pi}$ is not available, we approximate it using K_2 sampled tours $\pi_1, \dots, \pi_{K_2} \sim p_{\theta(\lambda)}(\cdot | s, \mathcal{E})$:

$$R_\lambda^{(1)}(\mathcal{E}) \approx \max_{k=1, \dots, K_2} R_\lambda(\pi_k). \quad (18)$$

A baseline $b_\lambda^{(1)}(s_i)$ for the selection-head is formed by averaging $R_\lambda^{(1)}$ over K_1 samples while a baseline $b_\lambda^{(2)}(s_i, \mathcal{E}_{ij})$ for the routing-head is formed by averaging over the K_2 samples for a fixed s_i and \mathcal{E}_{ij} . Thus, we approximate the policy gradients with

$$\nabla J_1(\tilde{\theta}) \approx \frac{1}{BK_1} \sum_{i,j=1}^{B,K_1} A_{ij}^{(1)} \nabla_{\tilde{\theta}} \log(q_{\tilde{\theta}}(\mathcal{E}_{ij} | s_i)),$$

$$\nabla J_2(\theta) \approx \frac{1}{BK_1 K_2} \sum_{i,j,k=1}^{B,K_1,K_2} A_{ijk}^{(2)} \nabla_\theta \log(p_\theta(\pi_{ijk} | s_i, \mathcal{E}_{ij})),$$

$$A_{ij}^{(1)} = R_\lambda^{(1)}(\mathcal{E}_{ij}) - b_\lambda^{(1)}(s_i),$$

$$A_{ijk}^{(2)} = R_\lambda^{(2)}(\pi_{ijk}) - b_\lambda^{(2)}(s_i, \mathcal{E}_{ij}).$$

(19)

We outline the training of GMS-DH in Algorithm 1.

In addition, we utilize a form of curriculum learning to speed up training for both models. We start by training on small graph sizes and then gradually increase the problem size. For GMS-DH in the multigraph setting, we also start by training the routing-head on simple graphs to ensure that the approximation (18) is accurate even during the initial epochs of multigraph training. Further details regarding the curriculum learning can be found in Appendix C.

Algorithm 1: One batch of REINFORCE for GMS-DH

Input: Preference distribution Λ , instance distribution S , batch size B , number of samples per instance head 1, K_1 , and head 2, K_2

- 1: Sample preference $\lambda \sim \Lambda$
 - 2: Sample instances $s_i \sim S, i = 1, \dots, B$
 - 3: Select edges $\mathcal{E}_{ij} \sim q_{\tilde{\theta}(\lambda)}(\cdot | s_i), j = 1, \dots, K_1$
 - 4: Sample tours $\pi_{ijk} \sim p_{\theta(\lambda)}(\cdot | s_i, \mathcal{E}_{ij}), k = 1, \dots, K_2$
 - 5: Calculate $R_\lambda^{(1)}(\mathcal{E}_{ij}), R_\lambda^{(2)}(\pi_{ijk}), b_\lambda^{(1)}(s_i), b_\lambda^{(2)}(s_i, \mathcal{E}_{ij})$
 - 6: Calculate gradients $\nabla J_1(\theta), \nabla J_2(\theta)$ with (19)
 - 7: $\tilde{\theta} \leftarrow \text{ADAM}(\tilde{\theta}, \nabla J_1(\tilde{\theta})), \theta \leftarrow \text{ADAM}(\theta, \nabla J_2(\theta))$,
-

5 Experimental Studies

In this section we show the empirical performance for our two proposed methods on several routing problems across multiple instance sizes and distributions. We compare against evolutionary algorithms, neural baselines and state-of-the-art single-objective heuristics.

5.1 Benchmarking Setup

Problems In the asymmetric simple graph case we consider two standard routing problems: The Multi-Objective Traveling Salesman Problem (MOTSP) and Multi-Objective Capacitated Vehicle Routing Problem (MOCVRP). Specifically, we consider bi-objective variants of these. In the MOTSP, we sample two distances for each node pair. These are summarized over the tour to yield the objective values. Regarding the distances, we consider both the TMAT (Kwon et al. 2021) and XASY distributions (Gaile et al. 2022), where the former obeys the triangle inequality and the latter does not - making it more difficult. For the MOCVRP, we sample one distance according to these distributions. We then let the first objective be given by the total distance of a tour and the second objective by the makespan, which is the longest trip for a single vehicle. This is a standard benchmark problem in literature (Lin, Yang, and Zhang 2022).

In the multigraph setting, we consider the Multigraph MOTSP (MGMOTSP) with two objectives, where we sample two-dimensional edge distances using distributions called FIX_x and FLEX_x . Here, x denotes the number of edges between each node pair. In the FLEX_x -distribution, we sample edge distances independently and remove edges which are dominated. In the FIX_x distribution we first sample edges independently, but then rearrange by sorting, so that the an edge that is best in one objective is the worst in the other objective. Thus, in the FIX_x -distribution there are always exactly x edges between each node pair, whereas FLEX_x has at most x edges.

In Appendix D, we provide more in-depth explanations of the problems and distributions. We also provide results on Euclidean problems in Appendix G.

Baselines For the MOTSP and MGMOTSP, we utilize linear scalarization together with strong single-objective methods in the form of LKH3 (Helsgaun 2017) and Google OR-tools (Perron and Furnon 2019). We also benchmark against

four Multi-Objective Evolutionary Algorithms (MOEAs): MOGLS (Ishibuchi and Murata 1998), MOEA/D (Zhang and Li 2007), NSGA-II (Deb et al. 2002) and NSGA-III (Blank, Deb, and Roy 2019). Below, we only show the results for the MOEA that performs best in each scenario.

Finally, we also design a neural baseline based on the MatNet-architecture (Kwon et al. 2021) as encoder and a preference-conditioned MP network as decoder. We call this MatNet-Based Model (MBM) and our motivation is that it is a method that can be used almost "off-the-shelf" by combining components from literature. In the multigraph setting, this architecture requires us to pre-process the input by pruning edges until we obtain a simple graph, which we do using linear scalarization following Proposition 1.

In Appendix B and E, we provide further details about the neural benchmark and MOEAs respectively. In Appendix G, we also show results for all MOEAs as well as some other weaker heuristics.

Model Settings We train all models for 200 epochs using 100 000 randomly generated instances per epoch with the ADAM optimizer (Kingma and Ba 2015). We use the batch size $B = 64$ and the learning-rate $\eta = 10^{-4}$. For GMS-EB we let the number of layers be $L = 6$, while GMS-DH has $L_1 = 5$ and $L_2 = 2$. For both models we set the embedding dimension to 128 and use 8 attention heads in the GREAT layers and MP decoders. Regarding the number of samples in the decoding, we set $K_1 = 4$ for the selection-decoder during training and $K_1 = 1$ during inference. In the routing-decoder, we always set K_2 to the problem size as customary in the POMO framework (Kwon et al. 2020). Finally, we augment the models during inference with a factor of 8. For MBM, this is done using the original MatNet-augmentation (Kwon et al. 2021), while for GMS we use the scaling-augmentation of Lischka et al. (2025).

Metrics We utilize the Hypervolume (HV) metric (Zitzler et al. 2003) to evaluate the performance of the methods. Formally, for a given set of points $S = \{y_1, \dots, y_n\} \subset \mathbb{R}^m$ and a reference point $r \in \mathbb{R}^m$ that is dominated by all points in S , the HV is defined as:

$$\text{HV}(S, r) = \Lambda \left(\bigcup_{i=1}^n [y_i, r] \right), \quad (20)$$

where Λ denotes the Lebesgue measure in \mathbb{R}^m , and $[y_i, r]$ represents the axis-aligned hyperrectangle bounded by y_i and r . Intuitively, a higher HV generally indicates better performance, since the points in the obtained pareto front are further from the reference.

We report the normalized HV, which is scaled to lie in the interval $[0, 1]$, averaged over 200 test instances. For the neural models we use 101 preferences during inference, which is also the number of subproblems for the benchmarks relying on scalarization. Apart from the HV, we provide the HV gap compared to the best-performing method as well as the inference time. In Appendix C, we also report some training times for the learning-based methods.

Hardware We conducted training and inference for the learning-based methods using a single NVIDIA Tesla A40

		TMAT50			TMAT100			XASY50			XASY100		
		HV	Gap	Time									
MOTSP	LKH	0.58	0.00%	(6.4m)	0.63	0.00%	(29m)	0.83	0.00%	(6.9m)	0.90	0.00%	(32m)
	OR Tools	0.54	6.13%	(29m)	0.59	7.12%	(2.5h)	0.77	7.25%	(24m)	0.85	6.06%	(1.8h)
	MOEA/D	0.53	9.51%	(3.7h)	0.50	20.9%	(13h)	0.73	12.68%	(3.6h)	0.70	22.22%	(13h)
	MBM	0.50	13.5%	(3.9s)	0.56	11.2%	(19s)	0.75	10.37%	(3.7s)	0.84	7.41%	(19s)
	MBM (aug)	0.52	10.2%	(27s)	0.58	9.17%	(2.4m)	0.76	8.28%	(27s)	0.85	6.34%	(2.4m)
	GMS-EB	<u>0.57</u>	<u>1.50%</u>	(25s)	<u>0.63</u>	<u>1.45%</u>	(3.6m)	0.81	2.94%	(25s)	<u>0.88</u>	<u>3.03%</u>	(3.6m)
	GMS-DH	0.57	2.36%	(4.1s)	0.62	2.76%	(20s)	0.80	4.12%	(3.9s)	0.86	4.87%	(20s)
	GMS-EB (aug)	0.57	1.14%	(3.3m)	0.63	1.13%	(29m)	0.82	2.06%	(3.3m)	0.88	2.76%	(28m)
	GMS-DH (aug)	0.57	1.76%	(28s)	0.62	2.19%	(2.6m)	<u>0.81</u>	<u>2.84%</u>	(28s)	0.87	3.85%	(2.6m)
			TMAT50			TMAT100			XASY50			XASY100	
MOCVRP	MOEA/D	0.41	13.98%	(24h)	0.19	58.70%	(76h)	0.65	13.88%	(24h)	0.42	47.23%	(83h)
	MBM	0.47	1.33%	(6.2s)	0.43	4.50%	(27s)	0.70	6.57%	(6.2s)	0.60	24.47%	(27s)
	MBM (aug)	0.47	0.99%	(41s)	0.44	3.29%	(3.3m)	0.72	4.13%	(42s)	0.64	19.60%	(3.4m)
	GMS-EB	<u>0.47</u>	<u>0.25%</u>	(36s)	<u>0.45</u>	<u>0.57%</u>	(4.2m)	0.74	1.89%	(36s)	0.79	1.23%	(4.3m)
	GMS-DH	0.47	0.76%	(6.8s)	0.45	1.46%	(32s)	0.72	4.13%	(6.6s)	0.77	3.60%	(33s)
	GMS-EB (aug)	0.47	0.00%	(5.0m)	0.45	0.00%	(33m)	0.75	0.00%	(4.9m)	0.80	0.00%	(48m)
	GMS-DH (aug)	0.47	0.36%	(47s)	0.45	0.79%	(4.3m)	<u>0.74</u>	<u>1.65%</u>	(47s)	<u>0.79</u>	<u>1.21%</u>	(4.7m)
		FLEX2-50			FLEX2-100			FIX2-50			FIX2-100		
MGMOTSP	LKH	0.90	0.00%	(6.3m)	0.94	0.00%	(31m)	0.92	0.00%	(6.3m)	0.95	0.00%	(30m)
	OR Tools	0.86	4.21%	(24m)	0.91	3.46%	(1.8h)	0.90	2.59%	(24m)	0.93	2.25%	(2.0h)
	MOEA/D	0.74	17.50%	(18h)	0.68	28.46%	(99h)	0.78	15.42%	(18h)	0.72	24.69%	(91h)
	MBM	0.86	5.21%	(13s)	0.91	3.72%	(44s)	0.90	2.46%	(13s)	0.93	2.41%	(44s)
	MBM (aug)	0.87	3.98%	(1.7m)	0.91	3.28%	(5.9m)	0.91	1.66%	(1.7m)	0.93	2.10%	(5.9m)
	GMS-EB	0.88	2.00%	(56s)	0.93	1.81%	(9.1m)	<u>0.91</u>	<u>1.27%</u>	(57s)	0.94	1.33%	(9.2m)
	GMS-DH	0.89	1.84%	(13s)	0.92	2.11%	(49s)	0.91	1.73%	(12s)	0.93	2.13%	(52s)
	GMS-EB (aug)	<u>0.89</u>	<u>1.50%</u>	(7.5m)	0.93	1.47%	(1.2h)	0.91	1.02%	(7.5m)	0.94	1.09%	(1.2h)
	GMS-DH (aug)	0.89	1.45%	(1.5m)	<u>0.93</u>	<u>1.61%</u>	(6.6m)	0.91	1.40%	(1.5m)	0.93	1.92%	(6.6m)
	GMS-DH PP	0.77	14.24%	(33s)	0.83	12.53%	(2.3m)	0.82	10.51%	(33s)	0.85	10.39%	(2.3m)

Table 1: MOTSP, MOCVRP and MGMOTSP with different instance sizes (50, 100) and distributions. Runtime is the total time for solving 200 instances. The best results (excluding LKH, our baseline) are in **bold** and the second best are underlined.

GPU with 48GB of VRAM. For the non-learning-based methods, evaluations were performed on an Intel Xeon Gold 6338 CPU and, to enable a more fair comparison, we report execution time based on solving multiple instances in parallel. Akin to Kwon et al. (2021), we set the number of parallel processes to 8.

5.2 Performance on Benchmark Problems

We show the performance of GMS together with the other methods in Table 1. Both variants of GMS outperform most benchmarks on all problems. On the MOCVRP they are the best performing methods, while only LKH outperform them on the MOTSP and MGMOTSP. This showcases that our architectures are generally applicable across a variety of distributions, instance sizes and problems. As for the baseline neural method, MBM, it performs quite well across many cases, especially on the MGMOTSP, but severely un-

der performs on some distributions, e.g., XASY100 for the MOCVRP.

However, MBM is usually slightly faster than GMS-DH, owing to the MatNet architecture being faster and more memory-efficient than GREAT (for a comparison, see the results by Lischka et al. (2025)). GMS-DH has a small advantage for the MGMOTSP with 50 nodes due to only encoding each multigraph once, but this is offset again for 100 nodes. Nonetheless, both GMS models remain efficient relative to the other benchmarks, despite the slower scaling of GMS-EB. In particular, GMS-DH as well as GMS-EB without augmentation are significantly faster than LKH.

Apart from the previously mentioned benchmarks, we also evaluate a variant of GMS-DH with Pre-Pruning (GMS-DH PP) applied before the encoder in the MGMOTSP setting. This pre-pruning is the same as for MBM, and the selection head is removed accordingly.

		TMAT200			XASY200		
		HV	Gap	Time	HV	Gap	Time
MOTSP	LKH	0.67	0.00%	(1.2h)	0.95	0.00%	(1.3h)
	OR Tools	0.62	7.89%	(6.5h)	0.90	4.46%	(4.0h)
	GMS-EB	0.66	1.86%	(17m)	0.92	2.78%	(17m)
	GMS-DH	0.65	3.59%	(1.0m)	0.90	5.22%	(1.0m)
		FLEX2-200			FIX2-200		
MGMOTSP	LKH	0.97	0.00%	(1.2h)	0.97	0.00%	(1.2h)
	OR Tools	0.94	2.53%	(3.9h)	0.95	1.73%	(4.0h)
	GMS-EB	0.95	1.74%	(50m)	0.96	1.34%	(50m)
	GMS-DH	0.95	2.27%	(2.2m)	0.94	2.56%	(2.2m)

Table 2: MOTSP and MGMOTSP for larger instances (zero-shot generalization). Performance over 100 instances.

The poor performance of GMS-DH PP in Table 1 highlights the importance of explicitly designing for the multigraph structure, even when a theoretically sound pruning strategy is available. Since GMS-DH PP requires re-running the encoder for each preference, it is approximately $3\times$ slower than GMS-DH. We also hypothesize that the pre-pruning step shifts the data distribution in a way that GMS-DH is ill-equipped to model, resulting in performance that is worse than MBM with the same pruning strategy. Indeed, in our experience GMS-DH PP tends to produce Pareto fronts with poor diversity, clustered around central preference regions

5.3 Zero-Shot Generalization

We also test our models on larger instances not seen during training, and report the results in Table 2. Both GMS-DH and GMS-EB remain competitive across both problems and all distributions in this zero-shot setting.

5.4 More Difficult Multigraph Problem

Finally, we revisit one of the main motivations behind this work: routing for problems without clear a priori edge selection. Thus, we evaluate the performance on a more complex problem. Specifically, inspired by Ben Ticha et al. (2017), we consider an MGMOTSP with Time-Windows (MGMOTSPTW). Each edge is associated with a time and distance, while the objectives correspond to the number of violated time-windows and the total distance. Remark that, unlike the MGMOTSP, it is not clear in this case which edges can be pruned due to the more intricate time-window objective.

Besides MBM with linear pre-pruning and MOEAs, we benchmark against a simplified version of GMS-DH in order to ablate its ability to learn which edges are optimal. In this simplified version, we replace the selection-decoder with a simple function that removes edges with suboptimal linear cost. Compared to pre-pruning the multigraph before the encoder, this approach is smarter, as it removes the need to reencode. Furthermore, this simple variant actually performs quite well on the MGMOTSP, which we show and discuss in Appendix F.

We display the results for MGMOTSPTW in Table 3. Our two models are the best performing ones by quite a

		FLEX2-50			FIX2-50		
		HV	Gap	Time	HV	Gap	Time
MOEA/D		0.60	32.79%	(34h)	0.60	35.73%	(36h)
MBM		0.80	11.09%	(14s)	0.64	31.18%	(14s)
MBM (aug)		0.81	10.10%	(1.8m)	0.66	28.58%	(1.9m)
GMS-EB		0.89	0.97%	(60s)	0.93	0.55%	(59s)
GMS-DH		0.85	5.10%	(13s)	0.91	1.74%	(12s)
GMS-EB (aug)		0.90	0.00%	(7.9m)	0.93	0.00%	(7.9m)
GMS-DH (aug)		0.87	2.69%	(1.6m)	0.92	0.78%	(1.7m)
GMS-DH Simple		0.83	7.01%	(13s)	0.85	8.93%	(12s)

Table 3: MGMOTSPTW on the FLEX2 and FIX2 distributions with 50 nodes. Runtime is for solving 200 instances. In GMS-DH Simple, the selection-decoder is replaced with a simple pruning function.

large margin. Notably, vanilla GMS-DH also outperforms the simplified variant, which illustrates the value of learning to select beneficial edges in comparison to using a simple pruning heuristic.

6 Conclusion

In this paper, we propose two learning-based approaches for solving multi-objective routing problems, such as the MOTSP, on multigraphs and asymmetric graphs. Both methods utilize graph neural networks for encoding the graph structure but differ in their route construction strategies. The first method is edge-based and directly builds tours on the multigraph, while the second employs a two-stage decoding process, consisting of non-autoregressive pruning of the multigraph followed by route construction.

Empirical results show that both methods perform well across a variety of settings. While the edge-based model is simpler and usually demonstrates slightly superior performance, the second model is more scalable due to lower memory and runtime demands.

Finally, we highlight that our models can be valuable in all routing scenarios where multigraphs are appropriate, i.e., when there are multiple competing edges between each node pair. In future work, we plan to use our setup to address single-objective problems with hard constraints as well as stochastic variants.

Acknowledgements

This work was performed as a part of the research project “LEAR: Robust LEARNING methods for electric vehicle Route selection” funded by the Swedish Electromobility Centre (SEC). The computations were enabled by resources provided by the National Academic Infrastructure for Supercomputing in Sweden (NAISS) at Chalmers e-Commons partially funded by the Swedish Research Council through grant agreement no. 2022-06725. Through the affiliation of F.R., the work was also partially supported by the Wallenberg AI, Autonomous Systems and Software Program (WASP) funded by the Knut and Alice Wallenberg Foundation.

References

- Beke, L.; Weisz, M.; and Chen, J. 2021. A Comparison of Genetic Representations and Initialisation Methods for the Multi-objective Shortest Path Problem on Multigraphs. *SN Computer Science*, 2(3): 176.
- Bello, I.; Pham, H.; Le, Q. V.; Norouzi, M.; and Bengio, S. 2017. Neural Combinatorial Optimization with Reinforcement Learning. In *International Conference on Learning Representations*, volume 5.
- Ben Ticha, H.; Absi, N.; Feillet, D.; and Quilliot, A. 2017. Empirical Analysis for the VRPTW with a Multigraph Representation for the Road Network. *Computers & Operations Research*, 88: 103–116.
- Ben Ticha, H.; Absi, N.; Feillet, D.; and Quilliot, A. A. 2019. Multigraph Modeling and Adaptive Large Neighborhood Search for the Vehicle Routing Problem with Time Windows. *Computers and Operations Research*, 104: 113–126.
- Bi, J.; Ma, Y.; Zhou, J.; Song, W.; Cao, Z.; Wu, Y.; and Zhang, J. 2024. Learning to Handle Complex Constraints for Vehicle Routing Problems. In *Advances in Neural Information Processing Systems*, volume 37.
- Blank, J.; and Deb, K. 2020. pymoo: Multi-Objective Optimization in Python. *IEEE Access*, 8: 89497–89509.
- Blank, J.; Deb, K.; and Roy, P. C. 2019. Investigating the Normalization Procedure of NSGA-III. In *Evolutionary Multi-Criterion Optimization*, 229–240.
- Boyacı, B.; Dang, T. H.; and Letchford, A. N. 2021. Vehicle Routing on Road Networks: How good is Euclidean Approximation? *Computers & Operations Research*, 129: 105197.
- Capgemini Research Institute. 2023. The last-mile delivery challenge. <https://www.capgemini.com/wp-content/uploads/2019/01/Report-Digital-AS-Last-Mile-Delivery-Challenge1.pdf>.
- Chen, J.; Gong, Z.; Liu, M.; Wang, J.; Yu, Y.; and Zhang, W. 2024. Looking Ahead to Avoid Being Late: Solving Hard-Constrained Traveling Salesman Problem. ArXiv:2403.05318.
- Chen, J.; Wang, J.; Zhang, Z.; Cao, Z.; Ye, T.; and Chen, S. 2023a. Efficient Meta Neural Heuristic for Multi-Objective Combinatorial Optimization. In *Advances in Neural Information Processing Systems*, volume 36.
- Chen, J.; Zhang, Z.; Cao, Z.; Wu, Y.; Ma, Y.; Ye, T.; and Wang, J. 2023b. Neural Multi-Objective Combinatorial Optimization with Diversity Enhancement. In *Advances in Neural Information Processing Systems*, volume 37.
- Chen, X.; and Tian, Y. 2019. Learning to Perform Local Rewriting for Combinatorial Optimization. In Wallach, H.; Larochelle, H.; Beygelzimer, A.; d'Alché-Buc, F.; Fox, E.; and Garnett, R., eds., *Advances in Neural Information Processing Systems*, volume 32. Curran Associates, Inc.
- Choo, E. U.; and Atkins, D. R. 1983. Proper Efficiency in Nonconvex Multicriteria Programming. *Mathematics of Operations Research*, 8(3): 467–470.
- Deb, K.; Pratap, A.; Agarwal, S.; and Meyarivan, T. 2002. A Fast and Elitist Multiobjective Genetic Algorithm: NSGA-II. *IEEE Transactions on Evolutionary Computation*, 6(2): 182–197.
- Drakulic, D.; Michel, S.; and Andreoli, J.-M. 2025. GOAL: A Generalist Combinatorial Optimization Agent Learner. In *International Conference on Learning Representations*, volume 13.
- Drakulic, D.; Michel, S.; Mai, F.; Sors, A.; and Andreoli, J.-M. 2023. BQ-NCO: Bisimulation Quotienting for Efficient Neural Combinatorial Optimization. In *Advances in Neural Information Processing Systems*, volume 37.
- Ehrgott, M. 2005. *Multicriteria Optimization*. Springer Berlin, Heidelberg.
- Ehrgott, M.; and Gandibleux, X. 2000. A survey and Annotated Bibliography of Multiobjective Combinatorial Optimization. *OR-Spektrum*, 22(4): 425–460.
- Fan, M.; Wu, Y.; Cao, Z.; Song, W.; Sartoretti, G.; Liu, H.; and Wu, G. 2025. Conditional Neural Heuristic for Multi-objective Vehicle Routing Problems. *IEEE Transactions on Neural Networks and Learning Systems*, 36(3): 4677–4689.
- Fu, Z.-H.; Qiu, K.-B.; and Zha, H. 2021. Generalize a Small Pre-trained Model to Arbitrarily Large TSP Instances. In *Proceedings of the AAAI Conference on Artificial Intelligence*, volume 35.
- Gaile, E.; Draguns, A.; Ozoliņš, E.; and Freivalds, K. 2022. Unsupervised Training for Neural TSP Solver. In *Learning and Intelligent Optimization*.
- Garaix, T.; Artigues, C.; Feillet, D.; and Josselin, D. 2010. Vehicle Routing Problems with Alternative Paths: An Application to On-Demand Transportation. *European Journal of Operational Research*, 204(1): 62–75.
- Helsgaun, K. 2017. An Extension of the Lin-Kernighan-Helsgaun TSP Solver for Constrained Traveling Salesman and Vehicle Routing Problems. Technical report, Roskilde University.
- Hottung, A.; and Tierney, K. 2020. Neural Large Neighborhood Search for the Capacitated Vehicle Routing Problem. In *24th European Conference on Artificial Intelligence (ECAI 2020)*.
- Hudson, B.; Li, Q.; Malencia, M.; and Prorok, A. 2022. Graph Neural Network Guided Local Search for the Traveling Salesperson Problem. In *International Conference on Learning Representations*.
- Ishibuchi, H.; and Murata, T. 1998. A Multi-Objective Genetic Local Search Algorithm and its Application to Flowshop Scheduling. *IEEE Transactions on Systems, Man, and Cybernetics, Part C*, 28(3): 392–403.
- Jaszkievicz, A. 2002. Genetic local search for multi-objective combinatorial optimization. *European Journal of Operational Research*, 137(1): 50–71.
- Jin, Y.; Ding, Y.; Pan, X.; He, K.; Zhao, L.; Qin, T.; Song, L.; and Bian, J. 2023. Pointerformer: Deep Reinforced Multi-Pointer Transformer for the Traveling Salesman Problem. In *Proceedings of the AAAI Conference on Artificial Intelligence*, volume 37.

- Joshi, C. K.; Laurent, T.; and Bresson, X. 2019. An Efficient Graph Convolutional Network Technique for the Travelling Salesman Problem. ArXiv:1906.01227.
- Kingma, D. P.; and Ba, J. 2015. Adam: A Method for Stochastic Optimization. In *International Conference on Learning Representations*, volume 3.
- Kool, W.; van Hoof, H.; and Welling, M. 2018. Attention, Learn to Solve Routing Problems! In *International Conference on Learning Representations*, volume 7.
- Kwon, Y.-D.; Choo, J.; Kim, B.; Yoon, I.; Gwon, Y.; and Min, S. 2020. POMO: Policy Optimization with Multiple Optima for Reinforcement Learning. In *Advances in Neural Information Processing Systems*, volume 33.
- Kwon, Y.-D.; Choo, J.; Yoon, I.; Park, M.; Park, D.; and Gwon, Y. 2021. Matrix Encoding Networks for Neural Combinatorial Optimization. In *Advances in Neural Information Processing Systems*, volume 34.
- Lacomme, P.; Prins, C.; and Sevaux, M. 2006. A genetic algorithm for a bi-objective capacitated arc routing problem. *Computers & Operations Research*, 33(12): 3473–3493.
- Lai, D. S.; Caliskan Demirag, O.; and Leung, J. M. 2016. A Tabu Search Heuristic for the Heterogeneous Vehicle Routing Problem on a Multigraph. *Transportation Research Part E: Logistics and Transportation Review*, 86: 32–52.
- Legrand, C.; Cattaruzza, D.; Jourdan, L.; and Kessaci, M.-E. 2025. Improving Neighborhood Exploration into MOEA/D Framework to Solve a Bi-Objective Routing Problem. *International Transactions in Operational Research*, 32(1): 117–143.
- Li, K.; Zhang, T.; and Wang, R. 2021. Deep Reinforcement Learning for Multiobjective Optimization. *IEEE Transactions on Cybernetics*, 51(6): 3103–3114.
- Lin, X.; Yang, Z.; and Zhang, Q. 2022. Pareto Set Learning for Neural Multi-Objective Combinatorial Optimization. In *International Conference on Learning Representations*, volume 10.
- Lischka, A.; Rydin, F.; Wu, J.; Chehreghani, M. H.; and Kulcsár, B. 2025. A GREAT Architecture for Edge-Based Graph Problems Like TSP. ArXiv:2408.16717.
- Liu, S.; Chen, J.; and Weiszer, M. 2022. Multi-objective Multigraph A* Search with Learning Heuristics based on Node Metrics and Graph Embedding. In *IEEE International Conference on Intelligent Systems*, volume 11.
- Lu, H.; Zhang, X.; and Yang, S. 2020. A Learning-based Iterative Method for Solving Vehicle Routing Problems. In *International Conference on Learning Representations*.
- Lu, Y.; Di, Z.; Li, B.; Liu, S.; Qian, H.; Yang, P.; Tang, K.; and Zhou, A. 2024. Towards Geometry-Aware Pareto Set Learning for Neural Multi-Objective Combinatorial Optimization. ArXiv:2405.08604.
- Maggioni, F.; Perboli, G.; and Tadei, R. 2014. The Multi-path Traveling Salesman Problem with Stochastic Travel Costs: Building Realistic Instances for City Logistics Applications. *Transportation Research Procedia*, 3: 528–536.
- Navon, A.; Shamsian, A.; Chechik, G.; and Fetaya, E. 2021. Learning the Pareto Front with Hypernetworks. In *International Conference on Learning Representations*, volume 9.
- Perron, L.; and Furnon, V. 2019. OR-Tools. <https://developers.google.com/optimization/>.
- Qiu, R.; Sun, Z.; and Yang, Y. 2022. DIMES: A Differentiable Meta Solver for Combinatorial Optimization Problems. In *Advances in Neural Information Processing Systems*, volume 35.
- Santiyuda, G.; Wardoyo, R.; Pulungan, R.; and Yu, V. F. 2024. Multi-Objective Reinforcement Learning for Bi-Objective Time-Dependent Pickup and Delivery Problem with Late Penalties. *Engineering Applications of Artificial Intelligence*, 128: 107381.
- Sun, Z.; and Yang, Y. 2023. DIFUSCO: Graph-based Diffusion Solvers for Combinatorial Optimization. In *Advances in Neural Information Processing Systems*, volume 37.
- Tadei, R.; Perboli, G.; and Perfetti, F. 2017. The Multi-Path Traveling Salesman Problem with Stochastic Travel Costs. *EURO Journal on Transportation and Logistics*, 6(1): 3–23.
- Tikani, H.; Setak, M.; and Demir, E. 2021. Multi-Objective Periodic Cash Transportation Problem with Path Dissimilarity and Arrival Time Variation. *Expert Systems with Applications*, 164: 114015.
- Vaswani, A.; Shazeer, N.; Parmar, N.; Uszkoreit, J.; Jones, L.; Gomez, A. N.; Kaiser, L. u.; and Polosukhin, I. 2017. Attention is All you Need. In *Advances in Neural Information Processing Systems*, volume 30.
- Vinyals, O.; Fortunato, M.; and Jaitly, N. 2015. Pointer Networks. In *Advances in Neural Information Processing Systems*, volume 28.
- Weiszer, M.; Burke, E. K.; and Chen, J. 2020. Multi-objective Routing and Scheduling for Airport Ground Movement. *Transportation Research Part C: Emerging Technologies*, 119: 102734.
- Wu, H.; Wang, J.; and Zhang, Z. 2020. MODRL/D-AM: Multiobjective Deep Reinforcement Learning Algorithm Using Decomposition and Attention Model for Multi-objective Optimization. In *Artificial Intelligence Algorithms and Applications*.
- Ye, H.; Wang, J.; Liang, H.; Cao, Z.; Li, Y.; and Li, F. 2024. GLOP: Learning Global Partition and Local Construction for Solving Large-scale Routing Problems in Real-time. In *Proceedings of the AAAI Conference on Artificial Intelligence*, volume 38.
- Zhang, Q.; and Li, H. 2007. MOEA/D: A Multiobjective Evolutionary Algorithm Based on Decomposition. *IEEE Transactions on Evolutionary Computation*, 11(6): 712–731.
- Zhang, Z.; Wu, Z.; Zhang, H.; and Wang, J. 2021. Meta-Learning-Based Deep Reinforcement Learning for Multiobjective Optimization Problems. *IEEE Transactions on Neural Networks and Learning Systems*, 34: 7978–7991.
- Zhou, Y.; Kong, L.; and Wang, H. 2025. A Multiobjective Edge-Based Learning Algorithm for the Vehicle Routing Problem with Time Windows. *Information Sciences*, 715: 122223.

Zitzler, E.; Thiele, L.; Laumanns, M.; Fonseca, C.; and da Fonseca, V. 2003. Performance Assessment of Multi-objective Optimizers: an Analysis and Review. *IEEE Transactions on Evolutionary Computation*, 7(2): 117–132.

A Extended Related Work

In this section, we complement the literature review in the main text with a more thorough discussion of related work.

A.1 Single-Objective Learning for Routing

In the autoregressive paradigm, Vinyals, Fortunato, and Jaitly (2015) were early to propose learning solutions to the TSP. They utilized an oracle solver for supervised learning, and Bello et al. (2017) later introduced reinforcement learning for training. By using attention models and inherent symmetries in the problem, first Kool, van Hoof, and Welling (2018) and then Kwon et al. (2020) obtained greatly improved optimality gaps on various routing problems. Regarding asymmetric problems, Kwon et al. (2021) proposed MatNet, a mixed-attention architecture working on bi-partite graphs. More recent works are Jin et al. (2023); Drakulic et al. (2023); Chen et al. (2024); Bi et al. (2024). These papers have improved results, can handle constraints better and can scale to even larger problems than previously. Another recent notable contribution was made by Drakulic, Michel, and Andreoli (2025), who proposed a jointly trained generalist model to solve a multitude of combinatorial optimization problems, including examples from routing.

In the non-autoregressive category, some works are Joshi, Laurent, and Bresson (2019); Fu, Qiu, and Zha (2021); Qiu, Sun, and Yang (2022); Sun and Yang (2023). Typically, these methods require more sophisticated procedures than simple sampling in the decoding, such as Monte-Carlo tree search, to perform competitively, but scale better to large instances due to lower space and time complexity. Thus, an interesting recent work combining autoregressive and non-autoregressive construction to solve large instances (up to 10^5 nodes for the TSP) while maintaining performance is Ye et al. (2024).

Besides constructive approaches, *improvement-based* methods usually obtain great results, but with longer running-times, by refining initial solutions. Some examples are Chen and Tian (2019); Lu, Zhang, and Yang (2020); Hot-tung and Tierney (2020); Hudson et al. (2022).

A.2 Multi-Objective Learning for Routing

Early works treating MO routing using learning utilize multiple models, where one model is responsible for one preference between the objectives (Li, Zhang, and Wang 2021; Wu, Wang, and Zhang 2020). This quickly becomes infeasible as the number of models required grows exponentially with the number of objectives (Ehrgott 2005). Pareto-set learning for multi-objective routing using a single model was proposed by Lin, Yang, and Zhang (2022). They used the hyper-networks of Navon et al. (2021) to condition the decoder on the preference. Recent studies that feature improved results with a similar conditioning method include Fan et al. (2025) and Lu et al. (2024). An alternative approach is to use meta-learning to train a single model that can be quickly fine-tuned over a few steps to solve individual subproblems. Two representative works in this direction are Zhang et al. (2021) and Chen et al. (2023a).

Another significant recent work is that of Chen et al. (2023b), in which two diversity enhancement methods are

introduced. The authors combine these methods with both the meta-learning approach and hyper-network approach to achieve improved results.

Besides tackling asymmetric problems, our work is novel in the MO routing setting as most methods utilize autoregressive construction, while one of our models combine autoregressive and non-autoregressive construction.

A.3 Routing on Multigraphs

Successful approaches to tackle MO shortest path problems on multigraphs include genetic algorithms (Beke, Weiszer, and Chen 2021), A*-related methods (Weiszer, Burke, and Chen 2020) and hybrid approaches combining A* with learning (Liu, Chen, and Weiszer 2022). These methods all aim to find a Pareto set of shortest paths between two destinations.

For combinatorial routing problems such as VRPs on multigraphs, heuristics and exact solvers have been proposed. The first study in this regard was conducted by Garaix et al. (2010), who designed a simple heuristic and branch-and-price method for a single-objective on-demand transportation problem. Other works for single-objective constrained problems or multi-objective problems are Lai, Caliskan Demirag, and Leung (2016); Ben Ticha et al. (2019); Tikani, Setak, and Demir (2021). In addition, Ben Ticha et al. (2017) clearly concluded that a multigraph setup yields significantly lower costs compared to a simple graph representation for the capacitated VRP with time-windows. At the same time, the computation time increases significantly under this perspective, and the authors highlight the need for new heuristics.

B Architecture Details

Here, we highlight some of the main components in the model architectures that are not described in the main text.

B.1 Edge-Based Decoder in GMS-EB

In GMS-EB, we utilize an edge-based multi-pointer decoder which is inspired by Jin et al. (2023). Its mathematical formulation is the following. Given trainable weight matrices W_1, W_2, W_3, W_4 we form the query, representing the current routing context, as

$$q_t = W_1 e_{\pi_1} + W_2 e_{\pi_{t-1}} + \frac{1}{N} (W_3 e_{\text{graph}} + W_4 e_{\text{visited}}). \quad (21)$$

Here, e denotes an edge-embedding from the encoder, π_1 is the first visited edge and π_{t-1} the most recently visited edge. Moreover, we utilize an enhanced context in which e_{graph} is the sum of all embeddings in the graph and e_{visited} is the sum over the visited edges according to

$$e_{\text{visited}} = \sum_{t'=1}^{t-1} e_{\pi_{t'}}. \quad (22)$$

Let H be the number of heads/pointers. The score for edge l is formed according to

$$\alpha_l = \frac{1}{H} \sum_{h=1}^H \frac{1}{\sqrt{d_k}} (W_h^q q_t)^T (W_h^k k_l) - \text{Scalar cost}(l). \quad (23)$$

Note that the key k_l is the embedding e_l for the edge and d_k is its dimension. Similarly to the original article, we subtract a cost to speed up the exploration and ensure that costly edges are considered less favorable from the start. In our case, the cost is multi-objective so we must scalarize it. We find that both Chebyshev and linear scalarization work well for this purpose. The last step is to form the logits as

$$u_l = \begin{cases} c \tanh \alpha_l & \text{if } l \text{ connects current and unvisited node} \\ -\infty & \end{cases} \quad (24)$$

Finally, softmax is applied to transform the logits to probabilities.

In our case, we also preference-condition the decoder using a hyper-network. This is done by letting a multi-layer perceptron generate the weights W_1, W_2, W_3, W_4 and $(W_h^q, W_h^k)_{h=1}^H$.

B.2 Selection-Decoder in GMS-DH

The task of this decoder is to prune parallel edges in the intermediate stage of GMS-DH, leaving only one between each node pair. Initially, we apply L_3 GREAT NB layers on the edge embeddings from the encoder to obtain embeddings specialized for this task. In the experiments we set $L_3 = 2$. These layers are not preference conditioned and hence they do not need to be rerun for each preference. Next, given two nodes, we want to compute the probability of retaining each (directed) edge in between. For this purpose, we essentially utilize a multi-pointer score calculation similar to (23). Given a node pair (i, j) , and the set of edges in between, E_{ij} , let the query be the average embedding according to

$$q_{ij} = \frac{1}{|E_{ij}|} \sum_{l \in E_{ij}} e_l. \quad (25)$$

Moreover, let the key k_l be the embedding e_l . Then, form the score for edge l as

$$\alpha_l = \frac{1}{H} \sum_{h=1}^H \frac{1}{\sqrt{d_k}} (W_h^q q_{ij})^T (W_h^k k_l) - \text{Scalar cost}(l), \quad (26)$$

where $i = \text{start}(l)$ and $j = \text{end}(l)$. Again, note that we subtract a scalar cost to improve exploration. Also note that $(W_h^q, W_h^k)_{h=1}^H$ are generated by a hyper-network. Final edge probabilities are then computed using tanh-clipping and softmax as

$$u_l = c \tanh(\alpha_l), \quad (27)$$

$$p_l = \frac{\exp(u_l)}{\sum_{l' \in E_{ij}} \exp(u_{l'})}.$$

B.3 MatNet-Based Benchmark Model

We visualize this architecture in Figure 3. The encoder consists of L MatNet-layers (Kwon et al. 2021), while the decoder consists of an MP decoder (Jin et al. 2023) preference-conditioned with a hyper-network.

The MatNet-architecture operates on bipartite graphs. It utilizes mixed-score attention layers together with fully-connected layers and normalization as in standard trans-

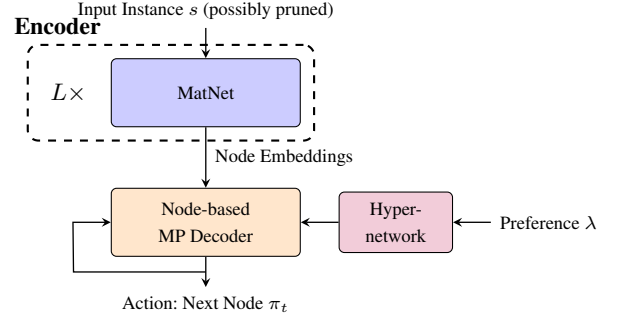


Figure 3: MatNet-Based Model (MBM)

former layers (Vaswani et al. 2017). These attention layers "mix" internally computed attention scores with external information from e.g. a distance matrix D . To accommodate the use of several distance matrices, D_1, \dots, D_f , in our multi-objective setting, we follow the idea in Appendix A of the original paper. That is, we mix the internal attention score with all distance matrices using an MLP with $f + 1$ inputs.

For the node-input to the initial MatNet-layer, in the absence of node-features we use zero-vectors for the "row" nodes and one-hot vectors for the "column" nodes, as in the original paper. If there are node features, e.g., demand in the MOCVRP, we use these as "row" input while keeping the one-hot "column" input. This allows us to augment each instance by sampling several one-hot combinations rather than scaling the instance as is done for GMS.

Lastly, we note that MatNet is not well-defined on multigraphs due to the fact that it utilizes the distance matrix to represent unique distances between nodes. It is possible to cast multigraphs into simple graphs, but not without increasing the number of nodes and edges drastically. Thus, we must pre-prune a multigraph before passing it through the encoder. This can be done with some sort of heuristic in the general case, but under linear scalarization and considering the MOTSP, an optimal pruning method is to remove edges with suboptimal scalarized cost. We utilize this pruning method for both multigraph problems. Moreover, it can be noted that the encoder needs to be rerun for each new preference, which results in a slower architecture than if the encoding is done once.

C Model Training

Here we outline the curriculum learning which we briefly discussed in the main text. We also present an analysis of training performance.

C.1 Curriculum Learning Details

For both GMS-EB and GMS-DH we utilize a simple curriculum learning approach, with the purpose to decrease training times and to improve performance on large problems. The idea is simple: we train on small instances before training on large instances with the same distribution.

For instances with 20 nodes, we do not use any such curriculum. For instances with 50 nodes we start by training

	#Params Enc.	#Params Dec.	Epoch SG	Epoch MG
MBM	2.38M	266K	4.7m	4.7m
GMS-DH	2.06M	1.08M	8.4m	24m
GMS-EB	1.98M	266K	51m	1.7h

Table 4: Number of parameters and time per epoch for the models. For GMS-DH, the parameters in the decoder refers to both decoders.

for 100 epochs on 20 nodes and then train on 50 nodes for 100 epochs. Finally, for instances with size 100, we start by training for 100 epochs on size 20. Then, for GMS-DH, we train for 50 epochs on size 50 and 50 epochs on size 100. As GMS-EB takes quite long to train for 100 nodes, we are satisfied with training for 100 epochs on size 50 for this model and then fine-tune it for 10 epochs on size 100, resulting in 210 epochs in total. Remark that our curriculum is quite arbitrary, but the model performance is not contingent on this exact setup.

Additionally, we start by training GMS-DH for 5 epochs (included in the first 100 epochs) on the XASY distribution with 20 nodes. This is because the selection-decoder relies on a reward signal from the routing-decoder. As such, we find that performance and rate of convergence improves if the routing-decoder is pre-trained on simple graphs to obtain a stable and accurate signal. We also find that stability increases if we freeze the parameters of the shared encoder with respect to the loss of the selection-decoder. That is, only the loss from the routing-decoder is utilized to calculate encoder gradients.

C.2 Training Times

Table 4 shows the number of parameters for the models as well as training time per epoch for one problem on a Simple Graph (SG) and Multigraph (MG). The SG problem is the MOTSP with 50 nodes, while the MG problem is the MG-MOTSP with 50 nodes and 2 parallel edges. It can be noted that GMS-EB takes a very long time to train, especially on multigraphs, while GMS-DH is more efficient and MBM is the most efficient. In fact, MBM is not affected by the multigraph representation as it works on pruned graphs.

We want to highlight that the training performance is a weakness of GMS. However, these models are very sample efficient, which is illustrated on examples with 20 nodes (that is, without curriculum learning) in Figure 4. Moreover, we try to remedy this weakness through the curriculum approach. When utilizing the curriculum learning, it is often enough to train on the small instance sizes to obtain a majority of performance and the rest is obtained after a few epochs of training on the larger instance. This can be seen in Figure 5, which showcases two examples with 50 nodes.

D Routing Problems and Distributions

In this section, we detail the distributions and routing problems which we solve.

D.1 Distributions

The following distributions for node distances are used across the problems on simple graphs.

- **EUC** - Euclidean. Here, we sample node coordinates uniformly and independently in the unit square. These are utilized to construct a distance matrix using the Euclidean distance. For a problem with m node distances (e.g., the MOTSP with m objectives) we sample m pairs of coordinates independently.
- **TMAT** - Asymmetric distance matrix obeying the triangle inequality (Kwon et al. 2021). The distance matrix is first populated with random independent elements and then post-processed until the triangle inequality is satisfied. For a problem with m distances, we sample m matrices independently.
- **XASY** - Extremely asymmetric distance matrix (Gaile et al. 2022). The distance matrix does not satisfy the triangle inequality. It is obtained by independently sampling each element uniformly between 0 and 1. Again, we sample all m matrices independently.

The following distributions are used for problems on multigraphs.

- **FLEX x** - Flexible number of edges between each node pair. Here we sample x vectors of dimension m representing edge attributes for edges between a node pair. Each attribute for each edge is sampled uniformly between 0 and 1. Then we remove dominated edges until only a Pareto set of edges remains.
- **FIX x** - Fixed number of edges between each node pair. We start by sampling x vectors in the same way as the FLEX-distribution. Then we sort each attribute so that no edge is dominated. For $m = 2$, we sort one attribute in descending order and one attribute in ascending order.

Note that neither FLEX x nor FIX x obeys the triangle inequality, although such an assumption holds for real instances. We highlight that these distributions are utilized since they are simple and easy to sample from, creating a more transparent picture of the model performance. Motivated by the fact that XASY seems more difficult to learn than TMAT, we hypothesize that the triangle inequality would contribute positively to model performance.

D.2 MOTSP

Problem Description In the multi-objective traveling salesman problem the goal is to visit all nodes/customers and return to the starting position. The Euclidean version of this problem has been widely treated in the learning-for-routing community, e.g., by Lin, Yang, and Zhang (2022) and Fan et al. (2025). In our case, we sample two distances, corresponding to the two objectives, between each pair of customers. The goal is to design a tour that minimizes the sum of the distances. A tour can start from any node.

Data Generation Edge distances are sampled according to the EUC, TMAT and XASY distributions above.

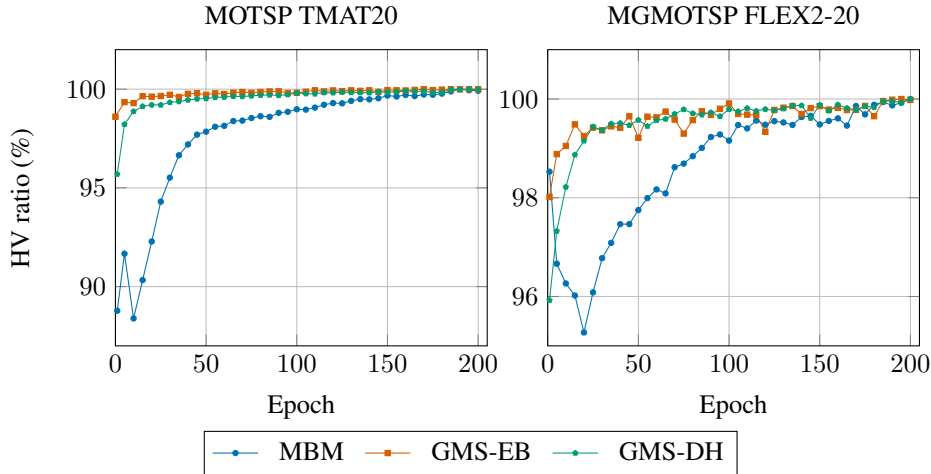


Figure 4: HV as percentage of best performance for models during training. GMS-EB and GMS-DH reach close to their final performance quickly and are more sample-efficient than MBM.

Model Details There are no node features for this problem, hence both the GREAT-based and MatNet-based encoders have the two distances as edge features, while the latter uses zero-vectors as "row" input.

Evaluation Details For all distributions, we utilize (15, 15), (30, 30) and (60, 60) as reference for HV calculation for 20, 50 and 100 nodes respectively. In the zero-shot experiments, we have (90, 90) as reference for 150 nodes and (120, 120) for 200 nodes.

D.3 MOCVRP

Problem Description In the multi-objective capacitated vehicle routing problem, a truck starts at a depot and must pick up goods from a specified number of customers. The vehicle has a fixed capacity while each customer has a demand. When the capacity is full, the vehicle must return to the depot. As many vehicles as required can be utilized to meet the demand of all customers.

Similarly to the TSP, this problem has been widely treated in the Euclidean setting using learning-based methods. As is common in the multi-objective setting (Lin, Yang, and Zhang 2022), we assume one objective is the traveled distance, while the other is the longest tour for a single vehicle (makespan). As such, each node pair is only associated with one distance.

Data Generation We assume that the capacity of the truck is 30, 40 and 50 for 20, 50 and 100 nodes respectively, while the demands are sampled uniformly from the set $\{1, \dots, 9\}$. This is the same setting as in e.g., Kool, van Hoof, and Welling (2018) and Lin, Yang, and Zhang (2022). Edge distances are sampled according to the EUC, TMat and XASY distributions.

Model Details In the decoding, we augment the routing context (represented by the query q_t) with the current load of the vehicle. For the GREAT-based encoders, we let the features of an edge be its distance as well as the demand

of the customer at the end. On the other hand, the MatNet-based encoders only utilize the distance as an edge-feature while the demand is used as a node feature.

Evaluation Details For all distributions, we utilize (15, 3), (40, 3) and (60, 3) as reference for HV calculation for the three considered instance sizes.

D.4 MG MOTSP

Problem Description As for the MOTSP, the goal of the multigraph MOTSP is to visit all nodes and return to the start. The only difference is that the underlying structure is a multigraph. Similarly, we define two distances for each node pair and these are associated with the objectives of the problem.

While this variant of the TSP on a multigraph has not been treated before to our knowledge (neither using learning nor other methods), some stochastic single-objective variants have been proposed by e.g., Tadei, Perboli, and Perfetti (2017) and Maggioni, Perboli, and Tadei (2014). Moreover, we believe that the MG MOTSP is a suitable benchmark problem for our solvers, as it is simple and easy to find good baselines for.

Data Generation We sample distances between the nodes according to the FLEX x and FIX x distributions.

Model Details As the MOTSP, the MG MOTSP lacks node features. Hence, we utilize the same setup for the models as in the MOTSP. Moreover, for the MatNet-based model, we sparsify the underlying multigraph given each preference before it is fed into the encoder. This is done by removing all edges with suboptimal linearly scalarized cost compared to a parallel edge. To make this pruning strategy exact, we train MBM using linear reward instead of the Chebyshev reward.

Evaluation Details For the FLEX x distribution, we utilize (15, 15), (30, 30) and (60, 60) as reference for instance sizes 20, 50 and 100, regardless of x . In the zero-shot experiments

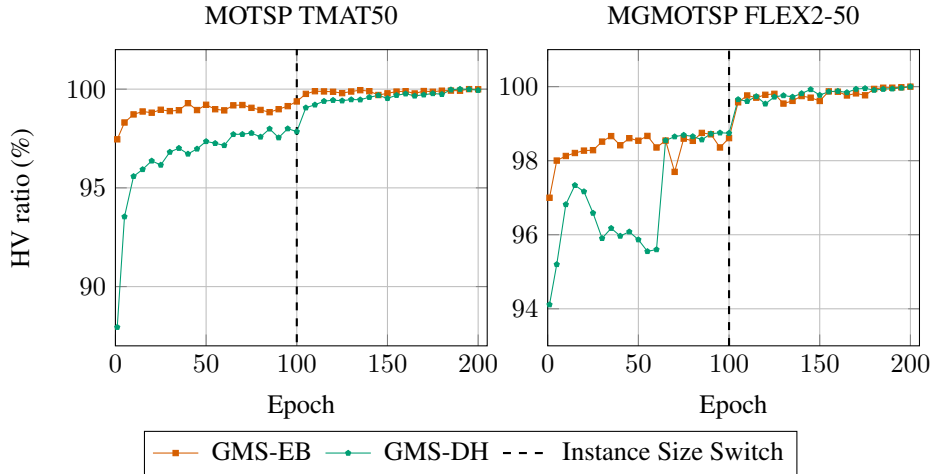


Figure 5: HV as percentage of best performance for GMS during training. It is enough to train on 20 nodes to obtain a majority ($\approx 98\%$) of the performance. After 5 epochs of training on instances with 50 nodes, the models reach $> 99.5\%$ of their final performance.

we set the references to $(90, 90)$ and $(120, 120)$ for $FLEX_x$ with 150 and 200 nodes. For FIX_x , the reference is given by (N, N) , where N is the node count.

D.5 MGMOTSPTW

Problem Description The goal in MGMOTSPTW is to create a tour that visits all customers and returns to the starting position. However, in this case we assume there is a fixed depot and that each customer/node is associated with a time-window. Preferably, the vehicle should arrive within the time-window for each customer. As such, we let one objective be the number of violated time-windows while the other is the traveled distance. Accordingly, each edge connecting two locations is associated with a travel time and a distance.

Multi-objective problems with similar objectives are fairly widespread in literature (Legrand et al. 2025), although not on multigraphs. In the multigraph framework, this problem is reminiscent of the vehicle routing problem with time-windows of Ben Ticha et al. (2017), but with a second objective that is the soft variant of the time-window constraint.

Data Generation Distances and travel times are sampled according to the $FLEX_x$ and FIX_x distributions. Additionally, we sample time-windows according to the "medium" distribution of Chen et al. (2024) and Bi et al. (2024). In this setting, time-windows are sampled uniformly and independently, which results in difficult instances where there is a true trade-off between optimal paths and paths satisfying the time-window constraint. We also argue that this premise is simple for initial evaluation of our models, especially in comparison to e.g., the "hard" instances of Chen et al. (2024), which test out-of-distribution generalization.

Further, we assume that the vehicle can depart immediately from each customer, i.e., that there is no service time, and that no waiting occurs, even if a vehicle arrives before

the starting time. The latter is for simplicity, as in general how long the vehicle should wait at a node is a decision in itself. We also argue that this assumption is fairly realistic.

Model Details In the decoder, we enhance the routing context with an embedding of the current time. In the encoder, the node features in this case are the starting time and end time of the service, while the edge features are distance and travel time. Consequently, we augment the input features of GREAT so that an edge is associated with its distance, travel time and the time-window of the ending node. As usual for MatNet, the node features are used as "row" inputs while the edge features are used in the distance matrix.

Note that in this case, pruning of the multigraph for MatNet is not obvious. For instance, removing an edge with a high travel time but low distance might not be optimal if traversing that edge would result in no violated time-windows anyway. For simplicity, we apply the same simple pruning method as for the MGMOTSP. That is, we form the scalarized cost of each edge using a linear combination of its travel time and distance, then we remove all edges apart from the best one. We also choose the linear reward instead of the Chebyshev reward for MBM.

Evaluation Details In this case, we let the reference value corresponding to the time-window violation be $N + 5$, while the reference value corresponding to the distance is the same as in the MGMOTSP case.

E Setup for MOEAs

As a base for the implementation of NSGA-II, NSGA-III and MOEA/D, we utilized Pymoo² (Blank and Deb 2020) and as a base for MOGLS, we utilized GeneticLocalSearch_TSP³ (Li, Zhang, and Wang 2021). For the former

²<https://pymoo.org/>

³https://github.com/kevin031060/Genetic_Local_Search_TSP

three, we limit the number of iterations to 1000 while the latter is limited to 10000. Additionally, local search strategies are a necessity for efficient usage of genetic algorithms in combinatorial optimization. For the MOTSP, we utilized the 2-opt heuristic of Jaskiewicz (2002), while we utilized the problem-specific local search and chromosome decoding strategy of Lacomme, Prins, and Sevaux (2006) for the MOCVRP.

However, in both cases we find that by accepting the best local move instead of just an improving one, the performance on large asymmetric problems improves substantially. As this affects the runtime negatively (due to the need to search through all moves), we limit the number of local moves in each search depending on the problem size. Additionally, for the algorithms not requiring preference weights for each individual (NSGA-II and NSGA-III), we must calculate such weights to compare the improvements. In the bi-objective case, this is done using the strategy of Lacomme, Prins, and Sevaux (2006) according to

$$\begin{aligned}\tilde{w}_1(S) &= (f_1(S) - f_1^{\min}) / (f_1^{\max} - f_1^{\min}), \\ \tilde{w}_2(S) &= (f_2(S) - f_2^{\min}) / (f_2^{\max} - f_2^{\min}), \\ w_1(S) &= \tilde{w}_1(S) / (\tilde{w}_1(S) + \tilde{w}_2(S)), \\ w_2(S) &= \tilde{w}_2(S) / (\tilde{w}_1(S) + \tilde{w}_2(S)),\end{aligned}\quad (28)$$

where S is the solution being improved and $f_i^{\min}, f_i^{\max}, i = 1, 2$ are minimum and maximum values for the respective objectives.

In the multigraph setting, we design our own setup to tailor the MOEAs. To start with, inspired by one representation from Beke, Weiszner, and Chen (2021) regarding shortest path problems, we let a chromosome for a tour be given by a permutation of the nodes multiplied with 100 added with the index of the edge to the next node. For example, in an MG-MOTSP with 2 parallel edges and 5 nodes, a chromosome might be

$$(101, 302, 201, 501, 402).$$

For the mutation operator, we randomly either change one edge or reverse a segment of the tour. For the crossover, we utilize an edge recombination operator. Regarding the local search, we use a variant of 2-opt where we again accept the best local move. A local move is defined by a standard 2-opt move with the nodes, together with new edge selections given the changed node order. This edge selection is found by choosing the edge with the lowest linearly scalarized cost between nodes that were previously not neighbors or have changed order.

We want to stress that the focus in this study is not to design evolutionary algorithms, we simply want baselines to compare against. We find that the proposed approach is somewhat efficient for small node counts, but performs quite badly for large graphs.

F Ablation Study

Here, we present additional results obtained by replacing the selection-decoder in GMS-DH with a simple pruning function that discards edges with suboptimal linearly scalarized cost. As shown in Section 5.4, this approach performs rather

	FLEX2-50		FIX2-50	
	HV	Gap	HV	Gap
GMS-DH Learned (Ch. Reward)	0.89	1.84%	0.91	1.73%
GMS-DH Learned (Lin. Reward)	0.88	2.74%	0.91	1.66%
GMS-DH Simple (Ch. Reward)	0.88	2.00%	0.90	1.82%
GMS-DH Simple (Lin. Reward)	0.88	2.65%	0.91	1.76%
GMS-DH PP (Lin. Reward)	0.77	14.24%	0.82	10.51%

Table 5: Ablation of the learned pruning in vanilla GMS-DH by replacing it with a simple pruning function. Results are for the MGMOTSP. The performance of GMS-DH PP from Table 1 is repeated for convenience.

poorly on the MGMOTSPTW. However, it is more reasonable to assume that it will yield good results for the MGMOTSP.

To ensure a fair comparison, we evaluate both learned pruning and simple pruning using linearly scalarized rewards and Chebyshev rewards. In the linear case, simple pruning is optimal by Proposition 1. Moreover, the learned pruning model is trained using $K_1 = 4$ edge selections per instance. Accordingly, we use $4\times$ more POMO samples when training the model with simple pruning to match the training budget.

Ablation results are shown in Table 5. For the MGMOTSP, simple and learned pruning perform quite similarly (although learned pruning shows a slight advantage under Chebyshev rewards for both distributions). Indeed, these results illustrate that it can be a smart approach to replace the selection-decoder in GMS-DH if a sound heuristic or exact pruning method is available. However, pruning after the encoder clearly outperforms pre-pruning (as used in GMS-DH PP), both in terms of solution quality and runtime, since pre-pruning requires reencoding the graph for each preference.

G Complementary Numerical Results

In this section, we show additional numerical results for more distributions, benchmarks and instance sizes.

G.1 Problems on Simple Graphs

Table 6 and 7 show results for the MOTSP and MOCVRP respectively. Apart from the benchmarks in the main text, we present the performance of three simple greedy heuristics on the MOTSP: Nearest Neighbor (NN), Nearest Insertion (NI) and Farthest Insertion (FI). Like LKH and OR-tools, these utilize the linear scalarization to transform the MO problem into single-objective subproblems. Additionally, we show results on Euclidean instances (EUC). For these, there are many existing models in literature and thus we replace MBM with the Conditional Neural Heuristic (CNH) of Fan et al. (2025). This model is augmented with the Euclidean augmentation of Lin, Yang, and Zhang (2022).

On the EUC distribution, our models are generally slightly worse than CNH. This is to be expected though, as a common pattern in previous studies is that architectures built for directed graph inputs perform worse on EUC than

those specialized for coordinate inputs (Lischka et al. 2025; Kwon et al. 2021).

G.2 Multigraph Problems

We display additional results for the MGMOTSP and MGMOTSPTW in Tables 8-11. As for the MOTSP, we include NN, NI and FI for MGMOTSP. In the case of MGMOTSPTW, we also include results for LKH and OR-tools when treating the problem as the MGMOTSP. That is, we neglect the time-windows and treat the time duration of each edge exactly as the distance. We call these methods implicit LKH and implicit OR-tools, as they implicitly minimize the time-window violations by reducing the time the tour takes. Additionally, for the MGMOTSP, we show results for FLEX5 and FIX5, i.e., when there are 5 parallel edges between each node pair.

G.3 Generalization to Larger Instances

In Tables 12-14, we report more generalization results for our methods in the MOTSP and MGMOTSP cases. Notably, even when introducing significantly more edges by testing on FLEX10 and FIX10, our methods remain competitive zero-shot.

	EUC20			EUC50			EUC100			
	HV	Gap	Time	HV	Gap	Time	HV	Gap	Time	
LKH	0.52	0.00%	(2.6m)	0.58	0.00%	(14m)	0.68	0.00%	(1.2h)	
OR Tools	0.51	0.97%	(2.0m)	0.57	1.83%	(15m)	0.67	1.57%	(1.3h)	
NN	0.46	11.44%	(1.9s)	0.51	11.42%	(7.1s)	0.63	8.23%	(25s)	
NI	0.47	8.53%	(11s)	0.52	9.97%	(1.8m)	0.63	7.82%	(12m)	
FI	0.50	3.44%	(13s)	0.55	5.79%	(2.1m)	0.65	4.96%	(14m)	
MOGLS	0.51	0.79%	(1.0h)	0.58	0.74%	(3.8h)	0.68	1.16%	(32h)	
NSGA-II	0.50	2.63%	(44m)	0.52	11.18%	(3.4h)	0.54	21.13%	(12h)	
NSGA-III	0.50	3.56%	(46m)	0.50	14.07%	(3.4h)	0.53	21.82%	(12h)	
MOEA/D	0.51	0.87%	(56h)	0.57	2.53%	(3.6h)	0.63	8.08%	(13h)	
CNH	0.51	1.16%	(6.5s)	0.57	1.84%	(7.1s)	0.67	1.89%	(25s)	
CNH (aug)	0.51	0.85%	(17s)	<u>0.57</u>	<u>1.26%</u>	(44s)	<u>0.67</u>	<u>1.45%</u>	(3.1m)	
GMS-EB	0.51	0.93%	(2.0s)	0.57	1.98%	(25s)	0.67	2.34%	(3.6m)	
GMS-DH	0.51	1.30%	(1.1s)	0.57	2.64%	(3.8s)	0.67	2.49%	(20s)	
GMS-EB (aug)	<u>0.51</u>	<u>0.81%</u>	(14s)	0.57	1.57%	(3.3m)	0.67	2.09%	(28m)	
GMS-DH (aug)	0.51	0.93%	(5.3s)	0.57	1.91%	(27s)	0.67	2.24%	(2.6m)	
		TMAT20			TMAT50			TMAT100		
LKH	0.58	0.00%	(2.3m)	0.58	0.00%	(6.4m)	0.63	0.00%	(29m)	
OR Tools	0.56	3.01%	(3.3m)	0.54	6.13%	(29m)	0.59	7.12%	(2.5h)	
NN	0.48	16.66%	(1.9s)	0.47	18.34%	(7.0s)	0.54	15.25%	(25s)	
NI	0.53	8.78%	(11s)	0.50	13.17%	(1.8m)	0.55	13.24%	(12m)	
FI	0.54	6.60%	(13s)	0.52	10.65%	(2.0m)	0.57	10.84%	(14m)	
MOGLS	0.54	7.72%	(20m)	0.40	30.90%	(2.7h)	0.38	40.03%	(19h)	
NSGA-II	0.57	2.17%	(44m)	0.51	12.91%	(3.5h)	0.47	25.98%	(12h)	
NSGA-III	0.57	2.87%	(45m)	0.50	14.54%	(3.5h)	0.46	27.53%	(13h)	
MOEA/D	0.57	1.43%	(56m)	0.53	9.51%	(3.7h)	0.50	20.93%	(13h)	
MBM	0.57	2.29%	(1.3s)	0.50	13.51%	(3.9s)	0.56	11.16%	(19s)	
MBM (aug)	0.58	0.96%	(5.6s)	0.52	10.17%	(27s)	0.58	9.17%	(2.4m)	
GMS-EB	0.58	0.88%	(2.2s)	<u>0.57</u>	<u>1.50%</u>	(25s)	<u>0.63</u>	<u>1.45%</u>	(3.6m)	
GMS-DH	0.58	1.08%	(1.3s)	0.57	2.36%	(4.1s)	0.62	2.76%	(20s)	
GMS-EB (aug)	0.58	0.67%	(15s)	0.57	1.14%	(3.3m)	0.63	1.13%	(29m)	
GMS-DH (aug)	<u>0.58</u>	<u>0.79%</u>	(5.6s)	0.57	1.76%	(28s)	0.62	2.19%	(2.6m)	
		XASY20			XASY50			XASY100		
LKH	0.75	0.00%	(2.3m)	0.83	0.00%	(6.9m)	0.90	0.00%	(32m)	
OR Tools	0.71	5.49%	(3.0m)	0.77	7.25%	(24m)	0.85	6.06%	(1.8h)	
NN	0.60	20.11%	(1.8s)	0.70	16.32%	(7.0s)	0.80	10.94%	(25s)	
NI	0.61	17.76%	(11s)	0.66	21.37%	(1.8m)	0.73	18.88%	(12m)	
FI	0.60	19.57%	(12s)	0.64	23.62%	(2.1m)	0.72	20.42%	(14m)	
MOGLS	0.65	13.23%	(19m)	0.51	39.16%	(2.6h)	0.47	47.82%	(19h)	
NSGA-II	0.72	4.06%	(44m)	0.70	15.63%	(3.5h)	0.64	29.74%	(13h)	
NSGA-III	0.71	4.56%	(45m)	0.70	16.64%	(3.5h)	0.63	30.13%	(13h)	
MOEA/D	0.73	2.68%	(56m)	0.73	12.68%	(3.6h)	0.70	22.22%	(13h)	
MBM	0.68	9.10%	(1.4s)	0.75	10.37%	(3.7s)	0.84	7.41%	(19s)	
MBM (aug)	0.70	5.86%	(5.5s)	0.76	8.28%	(27s)	0.85	6.34%	(2.4m)	
GMS-EB	0.73	1.95%	(2.3s)	0.81	2.94%	(25s)	<u>0.88</u>	<u>3.03%</u>	(3.6m)	
GMS-DH	0.73	2.37%	(1.9s)	0.80	4.12%	(3.9s)	0.86	4.87%	(20s)	
GMS-EB (aug)	0.74	1.30%	(15s)	0.82	2.06%	(3.3m)	0.88	2.76%	(28m)	
GMS-DH (aug)	<u>0.74</u>	<u>1.57%</u>	(5.8s)	<u>0.81</u>	<u>2.84%</u>	(28s)	0.87	3.85%	(2.6m)	

Table 6: MOTSP with different instance sizes (20, 50 and 100) and distributions.

	EUC20			EUC50			EUC100		
	HV	Gap	Time	HV	Gap	Time	HV	Gap	Time
MOGLS	0.23	3.35%	(4.1h)	0.17	37.39%	(26h)	0.00	100.00%	(108h)
NSGA-II	<u>0.23</u>	<u>0.13%</u>	(2.6h)	0.27	2.14%	(24h)	0.20	18.91%	(75h)
NSGA-III	0.23	0.21%	(2.7h)	0.26	2.91%	(25h)	0.20	21.23%	(75h)
MOEA/D	0.23	0.90%	(2.9h)	0.26	2.73%	(25h)	0.23	7.40%	(73h)
CNH	0.23	0.77%	(5.0s)	0.27	0.59%	(9.5s)	0.25	0.56%	(29s)
CNH (aug)	0.23	0.00%	(29s)	0.27	0.00%	(58s)	0.25	0.00%	(3.6m)
GMS-EB	0.23	0.30%	(3.4s)	0.27	0.44%	(33s)	0.25	0.56%	(4.1m)
GMS-DH	0.23	1.33%	(2.3s)	0.27	1.11%	(6.6s)	0.25	1.36%	(30s)
GMS-EB (aug)	<u>0.23</u>	<u>0.13%</u>	(22s)	<u>0.27</u>	<u>0.18%</u>	(4.7m)	<u>0.25</u>	<u>0.32%</u>	(54m)
GMS-DH (aug)	0.23	0.90%	(10s)	0.27	0.66%	(46s)	0.25	0.92%	(4.1m)
	TMAT20			TMAT50			TMAT100		
MOGLS	0.40	1.78%	(4.1h)	0.31	35.06%	(28h)	0.05	89.38%	(116h)
NSGA-II	0.40	1.38%	(2.7h)	0.36	23.04%	(23h)	0.13	71.72%	(76h)
NSGA-III	0.40	1.98%	(2.7h)	0.35	25.91%	(24h)	0.12	74.11%	(76h)
MOEA/D	0.39	2.59%	(3.0h)	0.41	13.98%	(24h)	0.19	58.70%	(76h)
MBM	0.40	1.14%	(2.4s)	0.47	1.33%	(6.2s)	0.43	4.50%	(27s)
MBM (aug)	0.40	0.86%	(10s)	0.47	0.99%	(41s)	0.44	3.29%	(3.3m)
GMS-EB	<u>0.40</u>	<u>0.25%</u>	(3.5s)	<u>0.47</u>	<u>0.25%</u>	(36s)	<u>0.45</u>	<u>0.57%</u>	(4.2m)
GMS-DH	0.40	0.64%	(2.5s)	0.47	0.76%	(6.8s)	0.45	1.46%	(32s)
GMS-EB (aug)	0.41	0.00%	(23s)	0.47	0.00%	(5.2m)	0.45	0.00%	(33m)
GMS-DH (aug)	0.40	0.32%	(10s)	0.47	0.36%	(47s)	0.45	0.79%	(4.3m)
	XASY20			XASY50			XASY100		
MOGLS	0.59	2.39%	(4.0h)	0.49	34.85%	(29h)	0.13	83.50%	(121h)
NSGA-II	<u>0.60</u>	<u>1.24%</u>	(2.7h)	0.55	27.19%	(24h)	0.28	64.39%	(85h)
NSGA-III	0.59	2.21%	(2.7h)	0.52	31.06%	(25h)	0.25	68.40%	(86h)
MOEA/D	0.59	3.24%	(3.0h)	0.65	13.88%	(24h)	0.42	47.23%	(83h)
MBM	0.57	5.95%	(2.3s)	0.70	6.57%	(6.2s)	0.60	24.47%	(27s)
MBM (aug)	0.59	3.06%	(10s)	0.72	4.13%	(42s)	0.64	19.60%	(3.4m)
GMS-EB	0.60	1.44%	(3.5s)	0.74	1.89%	(36s)	0.79	1.23%	(4.3m)
GMS-DH	0.58	3.40%	(2.4s)	0.72	4.13%	(6.6s)	0.77	3.60%	(33s)
GMS-EB (aug)	0.61	0.00%	(23s)	0.75	0.00%	(5.0m)	0.80	0.00%	(48m)
GMS-DH (aug)	0.60	1.29%	(10s)	<u>0.74</u>	<u>1.65%</u>	(47s)	<u>0.79</u>	<u>1.21%</u>	(4.7m)

Table 7: MOCVRP with different instance sizes (20, 50 and 100) and distributions.

	FLEX2-20			FLEX2-50			FLEX2-100		
	HV	Gap	Time	HV	Gap	Time	HV	Gap	Time
LKH	0.85	0.00%	(1.2m)	0.90	0.00%	(6.3m)	0.94	0.00%	(31m)
OR Tools	0.82	3.30%	(3.0m)	0.86	4.21%	(24m)	0.91	3.46%	(1.8h)
NN	0.74	13.34%	(1.9s)	0.81	10.38%	(7.1s)	0.88	6.71%	(25s)
NI	0.75	11.13%	(9.6s)	0.78	13.13%	(1.7m)	0.84	11.32%	(12m)
FI	0.75	11.98%	(12s)	0.77	14.30%	(2.0m)	0.83	12.20%	(14m)
MOGLS	0.71	16.29%	(1.9h)	0.49	45.84%	(29h)	0.34	64.38%	(129h)
NSGA-II	0.81	5.06%	(1.3h)	0.74	17.62%	(19h)	0.64	31.98%	(103h)
NSGA-III	0.80	5.82%	(1.3h)	0.74	18.48%	(19h)	0.63	33.01%	(104h)
MOEA/D	0.80	6.02%	(1.4h)	0.74	17.50%	(18h)	0.68	28.46%	(99h)
MBM	0.82	3.30%	(4.4s)	0.86	5.21%	(13s)	0.91	3.72%	(44s)
MBM (aug)	0.84	1.50%	(32s)	0.87	3.98%	(1.7m)	0.91	3.28%	(5.9m)
GMS-EB	0.83	1.61%	(4.0s)	0.88	2.00%	(56s)	0.93	1.81%	(9.1m)
GMS-DH	0.84	1.34%	(3.2s)	0.89	1.84%	(13s)	0.92	2.11%	(49s)
GMS-EB (aug)	<u>0.84</u>	<u>0.95%</u>	(34s)	<u>0.89</u>	<u>1.50%</u>	(7.5m)	0.93	1.47%	(1.2h)
GMS-DH (aug)	0.84	0.86%	(19s)	0.89	1.45%	(1.5m)	<u>0.93</u>	<u>1.61%</u>	(6.6m)
	FLEX5-20			FLEX5-50			FLEX5-100		
	HV	Gap	Time	HV	Gap	Time	HV	Gap	Time
LKH	0.93	0.00%	(1.3m)	0.95	0.00%	(6.4m)	0.97	0.00%	(30m)
OR Tools	0.91	1.51%	(2.9m)	0.93	2.01%	(25m)	0.96	1.60%	(1.8h)
NN	0.86	6.78%	(1.8s)	0.90	5.24%	(7.2s)	0.94	3.33%	(28s)
NI	0.88	5.48%	(9.5s)	0.89	6.41%	(1.7m)	0.92	5.45%	(12m)
FI	0.87	5.89%	(11s)	0.89	7.03%	(2.0m)	0.92	5.89%	(14m)
MOGLS	0.84	9.71%	(2.4h)	0.69	27.67%	(52h)	0.57	41.21%	(222h)
NSGA-II	0.88	5.19%	(1.4h)	0.80	16.61%	(31h)	0.71	26.79%	(215h)
NSGA-III	0.87	5.85%	(1.4h)	0.79	17.48%	(31h)	0.70	27.98%	(215h)
MOEA/D	0.88	5.07%	(1.5h)	0.82	13.49%	(30h)	0.76	22.05%	(210h)
MBM	0.90	2.38%	(4.4s)	0.93	2.48%	(13s)	0.96	1.71%	(45s)
MBM (aug)	0.92	1.26%	(32s)	0.93	2.12%	(1.7m)	0.96	1.44%	(5.9m)
GMS-EB	0.92	0.87%	(8.1s)	<u>0.94</u>	<u>1.08%</u>	(2.3m)	<u>0.96</u>	<u>1.11%</u>	(23m)
GMS-DH	0.92	1.03%	(3.5s)	0.94	1.64%	(16s)	0.96	1.66%	(1.3m)
GMS-EB (aug)	0.92	0.59%	(1.1m)	0.95	0.86%	(18m)	0.96	0.96%	(3.0h)
GMS-DH (aug)	<u>0.92</u>	<u>0.64%</u>	(23s)	0.94	1.31%	(2.2m)	0.96	1.45%	(9.9m)

Table 8: MGMOTSP on FLEX x with different instances sizes (20, 50 and 100) and number of edges (2, 5).

	FIX2-20			FIX2-50			FIX2-100		
	HV	Gap	Time	HV	Gap	Time	HV	Gap	Time
LKH	0.85	0.00%	(1.2m)	0.92	0.00%	(6.3m)	0.95	0.00%	(30m)
OR Tools	0.83	2.42%	(2.9m)	0.90	2.59%	(24m)	0.93	2.25%	(2.0h)
NN	0.77	9.86%	(1.9s)	0.86	6.34%	(7.1s)	0.91	4.23%	(25s)
NI	0.78	8.39%	(9.6s)	0.85	7.95%	(1.7m)	0.88	7.14%	(12m)
FI	0.78	9.23%	(11s)	0.84	8.82%	(2.0m)	0.88	7.89%	(14m)
MOGLS	0.74	13.68%	(1.9h)	0.65	29.64%	(29h)	0.54	42.73%	(122h)
NSGA-II	0.81	5.64%	(1.3h)	0.77	16.56%	(19h)	0.69	27.86%	(96h)
NSGA-III	0.80	6.85%	(1.3h)	0.75	18.79%	(19h)	0.66	30.17%	(95h)
MOEA/D	0.80	6.20%	(1.4h)	0.78	15.42%	(18h)	0.72	24.69%	(91h)
MBM	0.84	1.57%	(4.4s)	0.90	2.46%	(13s)	0.93	2.41%	(44s)
MBM (aug)	0.85	0.50%	(32s)	0.91	1.66%	(1.7m)	0.93	2.10%	(5.9m)
GMS-EB	0.84	1.46%	(3.9s)	<u>0.91</u>	<u>1.27%</u>	(57s)	<u>0.94</u>	<u>1.33%</u>	(9.2m)
GMS-DH	0.84	1.37%	(3.2s)	0.91	1.73%	(12s)	0.93	2.13%	(52s)
GMS-EB (aug)	0.85	0.99%	(28s)	0.91	1.02%	(7.5m)	0.94	1.09%	(1.2h)
GMS-DH (aug)	<u>0.85</u>	<u>0.82%</u>	(18s)	0.91	1.40%	(1.5m)	0.93	1.92%	(6.6m)
	FIX5-20			FIX5-50			FIX5-100		
	HV	Gap	Time	HV	Gap	Time	HV	Gap	Time
LKH	0.84	0.00%	(56s)	0.89	0.00%	(6.2m)	0.91	0.00%	(29m)
OR Tools	0.82	1.41%	(3.0m)	0.87	1.78%	(25m)	0.90	1.78%	(2.0h)
NN	0.79	5.97%	(1.9s)	0.85	4.22%	(7.2s)	0.88	3.11%	(25s)
NI	0.79	4.98%	9.8s)	0.84	5.27%	(1.7m)	0.86	5.24%	(12m)
FI	0.79	6.00%	(11s)	0.83	6.45%	(2.0m)	0.85	6.37%	(14m)
MOGLS	0.74	11.00%	(2.5h)	0.67	24.51%	(38h)	0.62	32.11%	(253h)
NSGA-II	0.79	5.96%	(1.5h)	0.72	18.65%	(32h)	0.63	30.45%	(216h)
NSGA-III	0.77	7.78%	(1.5h)	0.69	21.60%	(32h)	0.60	33.77%	(218h)
MOEA/D	0.79	5.44%	(1.5h)	0.77	13.45%	(31h)	0.71	22.40%	(230h)
MBM	0.82	1.45%	(4.4s)	0.87	2.34%	(13s)	0.89	1.94%	(44s)
MBM (aug)	0.83	0.47%	(32s)	0.87	1.82%	(1.7m)	0.90	1.69%	(5.9m)
GMS-EB	0.83	1.05%	(8.1s)	<u>0.88</u>	<u>1.03%</u>	(2.3m)	<u>0.90</u>	<u>1.08%</u>	(23m)
GMS-DH	0.82	1.75%	(3.5s)	0.86	2.96%	(16s)	0.88	3.44%	(1.3m)
GMS-EB (aug)	<u>0.83</u>	<u>0.77%</u>	(1.1m)	0.88	0.89%	(19m)	0.90	0.99%	(3.0h)
GMS-DH (aug)	0.83	1.21%	(23s)	0.86	2.38%	(2.2m)	0.89	2.98%	(9.8m)

Table 9: MGMOTSP on FIX x with different instances sizes (20, 50 and 100) and number of edges (2, 5).

	FLEX2-20			FLEX2-50		
	HV	Gap	Time	HV	Gap	Time
Implicit LKH	0.27	66.74%	(1.1m)	0.14	84.11%	(6.7m)
Implicit OR Tools	0.24	70.78%	(3.4m)	0.13	85.34%	(25m)
MOGLS	0.64	22.92%	(2.7h)	0.35	60.96%	(21h)
NSGA-II	0.69	16.55%	(2.4h)	0.51	43.47%	(35h)
NSGA-III	0.69	16.01%	(2.5h)	0.50	44.53%	(36h)
MOEA/D	0.75	9.19%	(2.7h)	0.60	32.79%	(34h)
MBM	0.72	12.89%	(4.9s)	0.80	11.09%	(14s)
MBM (aug)	0.73	11.98%	(34s)	0.81	10.10%	(1.8m)
GMS-EB	0.81	1.95%	(4.3s)	<u>0.89</u>	<u>0.97%</u>	(60s)
GMS-DH	0.80	3.37%	(3.3s)	0.85	5.10%	(13s)
GMS-EB (aug)	0.82	0.00%	(31s)	0.90	0.00%	(7.9m)
GMS-DH (aug)	<u>0.82</u>	<u>0.33%</u>	(20s)	0.87	2.69%	(1.6m)
GMS-DH Simple	0.76	8.18%	(3.3s)	0.83	7.01%	(13s)

Table 10: MGMOTSPTW on FLEX x with different instances sizes (20, 50).

	FIX2-20			FIX2-50		
	HV	Gap	Time	HV	Gap	Time
Implicit LKH	0.28	67.24%	(1.3m)	0.15	84.24%	(6.5m)
Implicit OR Tools	0.25	71.02%	(3.4m)	0.14	85.49%	(26m)
MOGLS	0.62	28.85%	(2.8h)	0.41	55.72%	(21h)
NSGA-II	0.73	15.93%	(2.7h)	0.56	39.66%	(35h)
NSGA-III	0.71	18.88%	(2.5h)	0.53	43.42%	(35h)
MOEA/D	0.74	14.99%	(2.8h)	0.60	35.73%	(36h)
MBM	0.53	38.64%	(4.9s)	0.64	31.18%	(14s)
MBM (aug)	0.54	38.10%	(35s)	0.66	28.58%	(1.9m)
GMS-EB	0.86	1.17%	(4.3s)	<u>0.93</u>	<u>0.55%</u>	(59s)
GMS-DH	0.85	2.47%	(3.4s)	0.91	1.74%	(12s)
GMS-EB (aug)	0.87	0.00%	(31s)	0.93	0.00%	(7.9m)
GMS-DH (aug)	<u>0.87</u>	<u>0.46%</u>	(20s)	0.92	0.78%	(1.7m)
GMS-DH Simple	0.76	12.07%	(3.2s)	0.85	8.93%	(12s)

Table 11: MGMOTSPTW on FIX x with different instances sizes (20, 50).

	EUC150			EUC200		
	HV	Gap	Time	HV	Gap	Time
LKH	0.73	0.00%	(1.6h)	0.76	0.00%	(3.0h)
OR Tools	0.72	1.38%	(1.7h)	0.75	1.24%	(3.5h)
CNH ZS	<u>0.72</u>	<u>2.04%</u>	(50s)	<u>0.74</u>	<u>2.22%</u>	(1.3m)
GMS-EB ZS	0.71	2.71%	(6.7m)	0.74	2.93%	(17m)
GMS-DH ZS	0.71	2.82%	(30s)	0.74	3.12%	(1.0m)
	TMAT150			TMAT200		
	HV	Gap	Time	HV	Gap	Time
LKH	0.65	0.00%	(39m)	0.67	0.00%	(1.2h)
OR Tools	0.60	7.57%	(3.3h)	0.62	7.89%	(6.5h)
GMS-EB ZS	0.64	1.64%	(6.7m)	0.66	1.86%	(17m)
GMS-DH ZS	<u>0.63</u>	<u>3.20%</u>	(30s)	<u>0.65</u>	<u>3.59%</u>	(1.0m)
	XASY150			XASY200		
	HV	Gap	Time	HV	Gap	Time
LKH	0.93	0.00%	(40m)	0.95	0.00%	(1.3h)
OR Tools	0.88	5.12%	(2.2h)	0.90	4.46%	(4.0h)
GMS-EB ZS	0.90	2.77%	(6.7m)	0.92	2.78%	(17m)
GMS-DH ZS	<u>0.88</u>	<u>5.10%</u>	(30s)	0.90	5.22%	(1.0m)

Table 12: MOTSP for instances with more nodes.

	FLEX10-100			FIX10-100		
	HV	Gap	Time	HV	Gap	Time
LKH	0.98	0.00%	(16m)	0.86	0.00%	(15m)
OR Tools	0.98	0.87%	(57m)	<u>0.84</u>	<u>1.63%</u>	(1.1h)
GMS-EB ZS	<u>0.98</u>	<u>0.90%</u>	(23m)	0.84	1.49%	(23m)
GMS-DH ZS	0.97	1.53%	(1.1m)	0.82	4.11%	(1.1m)

Table 13: MGMOTSP for instances with more edges. The GMS models are those trained for FLEX5-100 and FIX5-100.

	FLEX2-150			FLEX2-200		
	HV	Gap	Time	HV	Gap	Time
LKH	0.96	0.00%	(39m)	0.97	0.00%	(1.2h)
OR Tools	0.93	2.93%	(2.1h)	0.94	2.53%	(3.9h)
GMS-EB ZS	0.94	1.78%	(18m)	0.95	1.74%	(50m)
GMS-DH ZS	<u>0.94</u>	<u>2.17%</u>	(1.0m)	<u>0.95</u>	<u>2.27%</u>	(2.2m)
	FLEX5-150			FLEX5-200		
	HV	Gap	Time	HV	Gap	Time
LKH	0.98	0.00%	(39m)	0.98	0.00%	(1.2h)
OR Tools	<u>0.97</u>	<u>1.35%</u>	(2.1h)	<u>0.97</u>	<u>1.15%</u>	(4.1h)
GMS-EB ZS	0.97	1.05%	(45m)	0.97	1.02%	(2.1h)
GMS-DH ZS	0.96	1.86%	(1.7m)	0.96	2.03%	(3.5m)
	FIX2-150			FIX2-200		
	HV	Gap	Time	HV	Gap	Time
LKH	0.96	0.00%	(39m)	0.97	0.00%	(1.2h)
OR Tools	<u>0.94</u>	<u>1.96%</u>	(2.2h)	<u>0.95</u>	<u>1.73%</u>	(4.0h)
GMS-EB ZS	0.95	1.35%	(18m)	0.96	1.34%	(50m)
GMS-DH ZS	0.94	2.38%	(1.1m)	0.94	2.56%	(2.2m)
	FIX5-150			FIX5-200		
	HV	Gap	Time	HV	Gap	Time
LKH	0.92	0.00%	(37m)	0.93	0.00%	(1.2h)
OR Tools	<u>0.91</u>	<u>1.69%</u>	(2.5h)	<u>0.92</u>	<u>1.59%</u>	(4.5h)
GMS-EB ZS	0.92	1.02%	(46m)	0.92	0.98%	(2.1h)
GMS-DH ZS	0.89	3.99%	(1.7m)	0.89	4.46%	(3.5m)

Table 14: MGMOTSP for instances with more nodes.